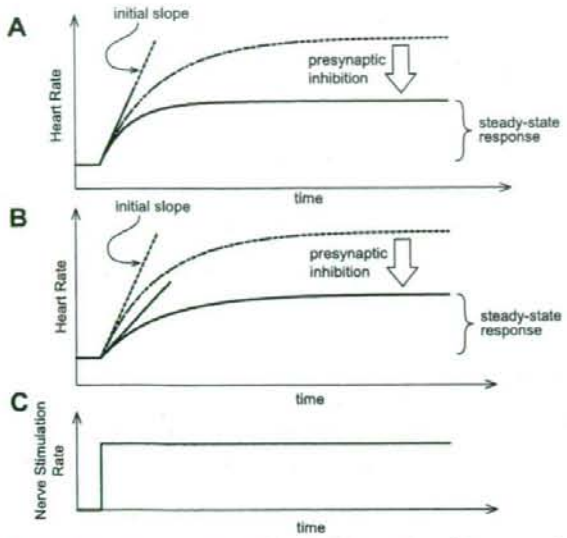

Fig. 1. Schematic representations of the possible operations of the presynaptic inhibition in heart rate (HR) step response to sympathetic nerve stimulation. The solid and dashed lines indicate the HR step response with and without the presynaptic inhibition, respectively. *A*: the presynaptic inhibition attenuates the steady-state response without affecting the initial slope of the response (a "limiter-like" operation). *B*: the presynaptic inhibition attenuates the steady-state response accompanied by a decrease in the initial slope in proportion to the attenuation of the steady-state response (an "attenuator-like" operation). Rapid effector response is maintained in the former but not in the latter. *C*: postulated nerve stimulation rate.

augmentation of presynaptic inhibition is an attenuator-like operation. A possible theoretical explanation for the difference in dynamic characteristics between the presynaptic α_2-adrenergic autoinhibition and the pharmacologic augmentation of the presynaptic inhibition will be proposed.

METHODS

Surgical Preparations

Animal care was in accordance with "Guiding Principles for the Care and Use of Animals in the Field of Physiological Sciences," approved by the Physiological Society of Japan. All protocols were reviewed and approved by the Animal Subject Committee of the National Cardiovascular Center. Japanese white rabbits, weighing 2.5–3.1 kg, were anesthetized by intravenous injection (2 ml/kg) of a mixture of urethane (250 mg/ml) and α-chloralose (40 mg/ml) and mechanically ventilated with oxygen-enriched room air. Tidal volume was set at 35 ml and the rate was adjusted between 35 and 40 cycles/min to be sufficient for suppressing spontaneous respiration. Supplemental doses of these anesthetics were administered by continuous intravenous infusion (1 $ml \cdot kg^{-1} \cdot h^{-1}$) into the marginal ear vein. Arterial pressure (AP) was monitored with a micromanometer catheter (model, Millar Instruments, Houston, TX) inserted into the right femoral artery. A catheter for drug administration was also placed in the right femoral vein. Sinoaortic denervation was performed bilaterally to minimize changes in systemic sympathetic activity via the arterial baroreflexes. The vagi were also sectioned bilaterally at the neck level to remove the vagal control on HR. The right inferior cardiac sympathetic nerve was exposed through a midline thoracotomy and sectioned. A pair of bipolar platinum electrodes was then attached to the cardiac end of the sectioned sympathetic nerve for stimulation (12, 13, 22, 23). The stimulation electrodes and nerve were secured with silicon glue (Kwik-Sil, World Precision Instruments, Sarasota, FL). Instantaneous HR was measured from the AP signal utilizing a cardiotachometer (Tachometer N4778, San-ei, Tokyo, Japan). Body temperature was maintained at 38°C with a heating pad throughout the experiment.

Experimental Procedures

Protocols. To estimate the transfer function from the sympathetic nerve stimulation to HR response, we employed a binary white noise stimulation signal with a switching interval of 5 s. The power spectrum of the sympathetic nerve stimulation rate was fairly constant up to 0.1 Hz and decreased to ~1/10 at 0.15 Hz. The upper frequency limit of the input power that covers the frequency range of physiological interest was determined based on our laboratory's previous studies (12, 23) and also preliminary experimental runs. Different sequences of binary white noise signals were used in different animals. Because HR is linearly related to cardiac output when stroke volume is unchanged, we chose HR as an output signal to understand sympathetic cardiovascular regulation. However, to rule out the possibility that the reciprocal relationship between R-R interval (RRI) and HR confounded the analytical results, we also calculated the transfer function using RRI as an output signal.

In *protocol 1* ($n = 6$), to examine the dynamic nature of the presynaptic α_2-adrenergic autoinhibition, we estimated the transfer function from dynamic sympathetic nerve stimulation to HR response from 20-min data obtained under control and α_2-adrenergic blockade conditions as follows. After recording the control data, an α_2-adrenergic antagonist yohimbine was administered intravenously with an initial bolus injection of 1 mg/kg, followed by continuous infusion at 0.1 $mg \cdot kg^{-1} \cdot h^{-1}$. The yohimbine bolus was equivalent to 10 h of infusion. The duration from the initiation of yohimbine administration until HR and AP reached new steady-state levels was ~15 min (35). We then repeated the 20-min dynamic sympathetic nerve stimulation and recorded the HR response under the α_2-adrenergic blockade condition.

In *protocol 2* ($n = 5$), to examine the effects of pharmacologic augmentation of the presynaptic α_2-adrenergic inhibition on the sympathetic HR control, we estimated the transfer function from dynamic sympathetic nerve stimulation to HR response before and during the administration of an α_2-adrenergic receptor agonist clonidine. Clonidine was administered intravenously at 0.3 and 1.5 $mg \cdot kg^{-1} \cdot h^{-1}$ in an increasing order. After 20-min baseline data collection, we started lower dose clonidine administration and waited for 15 min and then collected data for 20 min. Next, we started higher dose clonidine administration and waited for 15 min and then collected data for 20 min.

The stimulation rate of binary white noise was set at 0–1 Hz for *protocol 1*, and 0–5 Hz for *protocol 2*. Because we expected that blockade of the presynaptic α_2-adrenergic inhibition would augment, whereas activation of the inhibition would attenuate, the HR response, we set a higher stimulation rate for *protocol 2* than for *protocol 1*. The pulse width of sympathetic stimulation was set at 2 ms. The amplitude was set so that 5-Hz tonic sympathetic stimulation produced a HR increase of ~50 beats/min.

As a supplemental protocol, we performed the transfer function analysis using binary white noise signals of 0–1 Hz ($Bin_{0\text{-}1}$), 0–3 Hz ($Bin_{0\text{-}3}$), and 0–5 Hz ($Bin_{0\text{-}5}$) in a random order ($n = 5$). At least a 15-min interval was allowed between the 20-min dynamic sympathetic stimulation trials. The amplitude of sympathetic stimulation was set so that 1-Hz tonic sympathetic stimulation produced a HR increase of ~50 beats/min.

Medetomidine has higher affinity to α_2-adrenergic receptors over α_1-adrenergic receptors compared with clonidine (α_2/α_1 = 1,620:1 for medetomidine, 220:1 for clonidine) (28). However, a preliminary experiment indicated that medetomidine was not as effective as

clonidine to modulate the transfer function from dynamic sympathetic stimulation to HR. Accordingly, we examined the effects of clonidine or medetomidine on myocardial interstitial NE release in response to 5-Hz tonic stimulation (2.5 V, 2-ms pulse width) of the right cardiac sympathetic nerve in vagotomized rabbits. Two microdialysis probes were implanted in the myocardium of the left ventricular free wall. Ringer solution was perfused at 2 μl/min. After a 2-h equilibrium period, we collected 5-min dialysate samples to measure the dialysate NE concentration as an index of myocardial interstitial NE levels (14, 15). High-performance liquid chromatography with electrochemical detection was used to quantify the NE concentration. After the sympathetic stimulation was performed under the control condition, clonidine or medetomidine was intravenously administered (1.5 $mg \cdot kg^{-1} \cdot h^{-1}$). Fifteen minutes later, the sympathetic stimulation was performed under the drug administration condition. Then the drug administration was ceased. Forty-five minutes later, the sympathetic stimulation was performed under the recovery condition. We used different rabbits for clonidine and medatomidine trials. We pooled six dialysate data for statistical analysis.

Data Analysis

Data were digitized at 200 Hz utilizing a 12-bit analog-to-digital converter and stored on the hard disk of a dedicated laboratory computer system. Mean values for HR and AP during dynamic sympathetic nerve stimulation were calculated by averaging the respective data over the stimulation period.

The transfer function from dynamic sympathetic nerve stimulation to HR response was estimated by the following procedures. Twenty minutes of input data (stimulation command) and output data (HR) were resampled at 8 Hz. The resampled data were segmented into eight 50% overlapping bins consisting of 2,048 data points each. The segment length was 256 s. For each segment, the linear trend was subtracted, and a Hanning window was applied. Fast-Fourier transform was then performed to obtain the frequency spectrum of nerve stimulation rate [$N(f)$] and that of HR [$HR(f)$] (5). The power spectral density of the nerve stimulation rate [$S_{N \cdot N}(f)$], that of HR [$S_{HR \cdot HR}(f)$], as well as the cross-spectral density between these two signals [$S_{N \cdot HR}(f)$], were averaged over the eight segments. Finally, the transfer function [$H(f)$] from sympathetic nerve stimulation rate to HR response was calculated using the following equation (2, 21).

$$H(f) = \frac{S_{N \cdot HR}(f)}{S_{N \cdot N}(f)} \tag{1}$$

Transfer function parameters were determined by fitting a second-order, low-pass filter to the estimated transfer function, according to previous studies (12, 13, 23). The second-order, low-pass filter with a pure dead time [$G(f)$] is expressed as

$$G(f) = \frac{K}{1 + 2\zeta \frac{f}{f_N} j + \left(\frac{f}{f_N} j\right)^2} \exp(-2\pi f j L) \tag{2}$$

where K is a steady-state gain, f_N is natural frequency (in Hz), ζ is a damping ratio, L is pure dead time (in s), and j indicates an imaginary unit. A schematic explanation for these transfer function parameters is provided in the APPENDIX. To estimate the parameters, an iterative nonlinear least squares fitting was performed to minimize the following error function.

$$\text{error} = \frac{\sum_{k=1}^{n} |G(f) - H(f)|^2}{\sum_{i=1}^{n} |H(f)|^2}, \quad f = f_0 \times k \tag{3}$$

where f_0 is the fundamental frequency of the discrete Fourier transform, $f_0 = 1/256 = 0.004$ Hz, and k is a frequency index. The n represents the upper limit of the frequency index determined from the range of sufficient input power in the sympathetic nerve stimulation; $n = 40$, $f_0 \times n = 0.156$ Hz.

To quantify the linear dependence of the HR response on the sympathetic nerve stimulation, the magnitude-squared coherence function [$\gamma^2(f)$] was calculated by the following equation (2, 21).

$$\gamma^2(f) = \frac{|S_{N \cdot HR}(f)|^2}{S_{N \cdot N}(f) \cdot S_{HR \cdot HR}(f)} \tag{4}$$

The coherence value ranges from zero to unity. The unity coherence value indicates a perfect linear dependence between the input and output signals, whereas zero coherence indicates a total independence between the two signals.

To facilitate the intuitive understanding of the HR response to dynamic sympathetic nerve stimulation, we calculated the step response from the estimated transfer function. The step response was obtained from the time integral of the system impulse response derived from the inverse Fourier transform of the transfer function. The steady-state response was calculated by averaging the step response during the last 10 s of the 128-s response. To characterize the rising speed of the step response, the initial slope for the response was calculated as follows. An analysis of linear regression with a slope and an intercept was performed on the initial data points of the step response while varying the number of data points from 2 to 1,024. The maximum slope obtained was used as the initial slope of the response. The linear regression was performed, including the portion of the dead time. Although including the dead time reduced the maximum slope, the effect was small because the number of data points that yielded the maximum slope (~90 points) was much larger than that for the dead time (<10 points). The step response of RRI was also calculated from the corresponding transfer function from sympathetic nerve stimulation to RRI.

Statistics

All data are presented as means ± SE. In *protocol 1*, mean HR, AP, and transfer function parameters were compared before and during yohimbine administration by paired t-tests. In *protocol 2*, the data were compared among control, lower dose, and higher dose clonidine conditions using a repeated-measures ANOVA followed by Dunnett's test against the single control (8). In the supplemental protocol of the transfer function analysis, the data were compared among $Bin_{0\text{-}1}$, $Bin_{0\text{-}3}$, and $Bin_{0\text{-}5}$ stimulus conditions using a repeated-measures ANOVA followed by Tukey test for all pairwise comparisons. In the supplemental protocol of the NE measurement, baseline NE levels were compared before and during drug administration using a paired t-test. The NE levels during sympathetic stimulation were compared among control, drug administration, and recovery conditions using a repeated-measures ANOVA followed by Dunnett's test against the control condition. In all of the statistical procedures, the difference was considered significant at $P < 0.05$.

RESULTS

Figure 2*A* represents a typical recording obtained from *protocol 1*. We stimulated the cardiac sympathetic nerve according to a binary white noise signal and recorded HR response under control condition and during yohimbine administration. The presynaptic α_2-adrenergic negative feedback mechanism functioned under the control condition but not during yohimbine administration. HR changed dynamically in response to the random sympathetic nerve stimulation under both conditions. Yohimbine increased the magnitude of HR variation. The augmentation of sympathetic effect was also observed in the RRI response. Although yohimbine decreased the mean level of HR in this animal, changes in mean HR

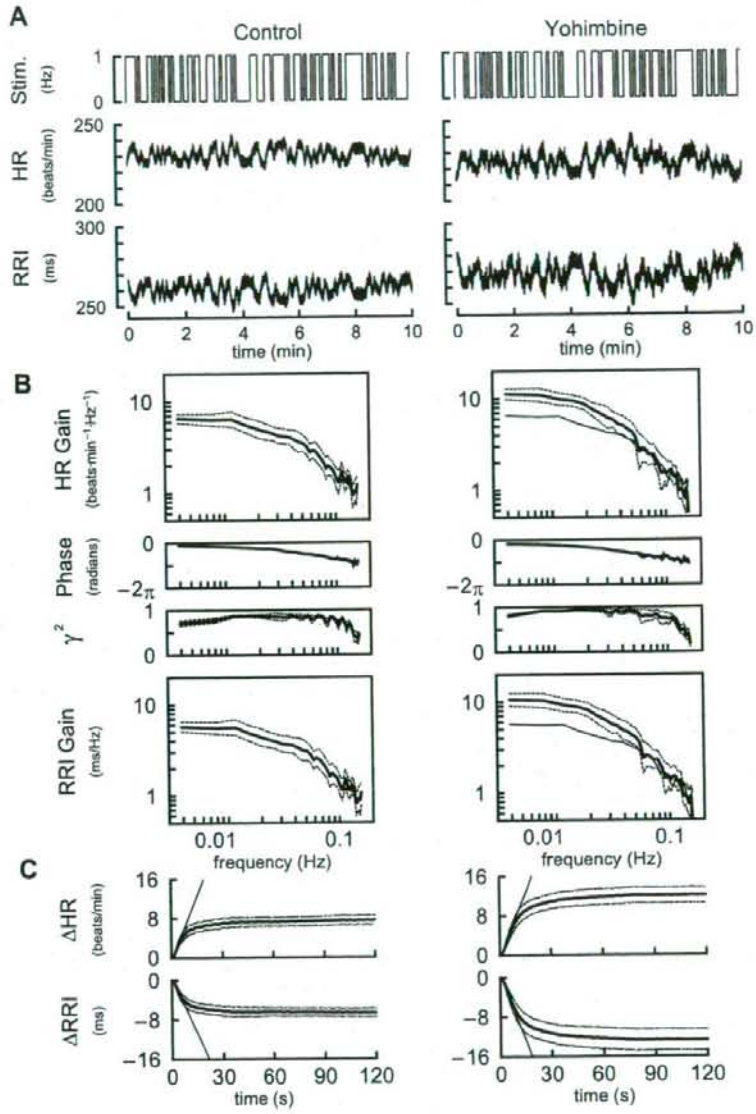

Fig. 2. *A:* representative recordings of cardiac sympathetic nerve stimulation rate (Stim; *top*), HR response (*middle*), and R-R interval (RRI) response (*bottom*) under conditions of control (*left*) and yohimbine administration (*right*) obtained in *protocol 1*. Yohimbine blocks the presynaptic α_2-adrenergic autoinhibition. The amplitude of HR variation and that of RRI variation become greater in the presence of yohimbine. *B:* transfer functions averaged over all animals in *protocol 1*. HR gain plots (*top*), phase plots (*second*), coherence functions (γ_2, *third*), and RRI gain plots (*bottom*). Yohimbine increases the dynamic gain in the frequency range between 0.004 and 0.04 Hz but not in the higher frequency range. The fine solid curve in the gain (*right*) duplicates the mean gain plot (*left*). *C:* step responses of HR (*top*) and RRI (*bottom*) calculated from the corresponding transfer functions. Yohimbine augments the steady-state response without affecting the initial slope of the response (fine oblique line). Bold, solid lines represent the mean, whereas dotted lines indicate means ± SE.

varied among the animals and were not significantly different between the control and yohimbine conditions.

Table 1 summarizes the mean HR and AP averaged from the six animals. The α_2-adrenergic blockade by yohimbine did not significantly affect the HR or AP before sympathetic nerve stimulation. Yohimbine also did not affect HR or AP significantly during the stimulation period.

Figure 2*B* illustrates the transfer functions averaged from the six animals in *protocol 1*. In the HR gain plots, the gain value was relatively constant <0.01 Hz and decreased >0.01 Hz, indicating low-pass filter characteristics of the HR response to sympathetic nerve stimulation. Yohimbine increased the HR gain from 7.1 ± 0.7 to 12.0 ± 1.7 beats·min^{-1}·Hz^{-1} at the lowest frequency of 0.004 Hz ($P < 0.05$). In contrast, yohimbine did not affect the HR gain value at 0.1 Hz (1.8 ± 0.4 vs. 1.7 ± 0.6 beats·min^{-1}·Hz^{-1}). The solid fine curve in the *right* panel duplicates the mean gain plot in the *left* panel as a reference. In the phase plots, the phase value approached zero radians at the lowest frequency and lagged with increasing frequency under both conditions. In the coherence function plots, the coherence was >0.8 in the frequency range from 0.01 to 0.08 Hz, suggesting that the HR response to sympathetic nerve stimulation in this frequency range can be explained reasonably well by linear dynamics for both conditions. Changes in the RRI gain plots were similar to those in the HR gain plots. Yohimbine increased the RRI gain from

Table 1. *Mean heart rate and arterial pressure before and during random stimulation of the cardiac sympathetic nerve*

	Control	Yohimbine
Heart rate, beats/min		
Before	259±15	244±13
During	264±15	254±17
Mean arterial pressure, mmHg		
Before	90±8	87±6
During	91±9	88±8

Values are means ± SE. Data were obtained after vagal and cardiac sympathetic nerves were cut. No statistically significant difference was detected between control vs. yohimbine values by paired *t*-tests.

6.0 ± 0.7 to 11.3 ± 1.9 ms/Hz at the lowest frequency of 0.004 ($P < 0.05$) but not at 0.1 Hz (1.8 ± 0.4 vs. 1.9 ± 0.8 ms/Hz). Given the inverse relationship between RRI and HR, the RRI phase plots (not shown) quite resembled to the corresponding HR phase plots except for the rotation by π radians.

Figure 2*C* represents the step responses of HR to sympathetic nerve stimulation calculated from the transfer functions shown in Fig. 2*B*. Yohimbine increased the steady-state response significantly (Table 2). The initial slope of the response, depicted by an oblique straight line, was not affected by yohimbine (Table 2). In the RRI step response, yohimbine augmented the steady-state response from −6.7 ± 0.9 to −12.6 ± 2.1 ms ($P < 0.05$) without affecting the initial slope (−0.71 ± 0.18 vs. −0.90 ± 0.23 ms/s).

Parameters of the transfer functions and step responses estimated in *protocol 1* are summarized in Table 2. The steady-state gain was significantly greater and the natural frequency was significantly lower in yohimbine condition compared with control. The damping coefficient and pure dead time did not differ significantly between the control and yohimbine conditions. Whereas the steady-state response was significantly increased by yohimbine, the initial slope of the step response was not significantly changed.

Figure 3*A* represents a typical recording of the sympathetic nerve stimulation and HR response obtained from *protocol 2*. The effects of α_2-adrenergic stimulation by clonidine were tested at two doses. Lower dose clonidine did not affect the magnitude of HR variation. Although lower dose clonidine decreased the mean HR in this animal, changes in the mean HR were not significantly different among the animals (Table 3). Higher dose clonidine significantly attenuated the magnitude of HR variation and also decreased mean HR. The attenuation of sympathetic effect was also observed in the RRI response during the high-dose clonidine administration.

Table 3 summarizes the mean HR and AP obtained from *protocol 2*. Higher dose, but not lower dose, clonidine significantly decreased the mean HR, both before and during cardiac sympathetic nerve stimulation. Clonidine did not affect mean AP significantly, before or during cardiac sympathetic nerve stimulation.

Figure 3*B* illustrates the transfer functions averaged from the five animals in *protocol 2*. Lower dose clonidine did not affect the transfer function significantly. In the HR gain plots, higher dose clonidine decreased the gain from 6.6 ± 0.9 to 2.7 ± 0.5 beats·min^{-1}·Hz^{-1} at the lowest frequency of 0.004 Hz ($P < 0.05$) and from 1.1 ± 0.2 to 0.5 ± 0.2 beats·min^{-1}·Hz^{-1} at the frequency of 0.1 Hz ($P < 0.05$). Higher dose clonidine did not affect the phase plot significantly. In the coherence function plots, the coherence was >0.8 in control and lower dose clonidine conditions and >0.7 in higher dose clonidine condition for the frequency range from 0.01 to 0.08 Hz, suggesting that the HR response to sympathetic nerve stimulation can be explained reasonably well by linear dynamics in all three conditions. Although relative change became smaller compared to the HR gain plots, the attenuation of transfer gain was also observed in the RRI gain plots. Higher-dose clonidine decreased the gain from 4.5 ± 0.7 to 2.8 ± 0.5 ms/Hz at the lowest frequency of 0.004 Hz ($P < 0.05$) and from 0.88 ± 0.19 to 0.04 ± 0.09 ms/Hz at the frequency of 0.1 Hz ($P < 0.05$).

Figure 3*C* represents the step responses of HR to sympathetic nerve stimulation calculated from the transfer functions shown in Fig. 3*B*. Lower dose clonidine did not affect either the steady-state response or the initial slope of the step response. In contrast, higher dose clonidine attenuated the steady-state response and also reduced the initial slope of the response. In the RRI step response, higher-dose clonidine attenuated the steady-state response from −4.9 ± 0.7 to −3.0 ± 0.6 ms ($P < 0.05$) with a significant reduction in the initial slope from −0.40 ± 0.07 to −0.23 ± 0.05 ms/s ($P < 0.05$).

Parameters of the transfer functions and step responses estimated in *protocol 2* are summarized in Table 4. The steady-state gain of the transfer function and the steady-state response of the corresponding step response were decreased by higher dose but not by lower dose clonidine. The initial slope of the step response was decreased by higher dose clonidine. The ratio of the steady-state response to the initial slope was unchanged. The natural frequency and the damping ratio of the transfer function were not affected by clonidine. The pure dead time of the transfer function was increased by lower dose, but not by higher dose, clonidine.

Figure 4*A* represents a typical recording of the sympathetic nerve stimulation and HR response obtained from the supplemental protocol. The binary white noise signals of the same sequence but different stimulus rate were applied. Increasing the stimulus rate augmented the magnitude of HR variation and increased mean HR. The increase was not proportional to the increase in the stimulus rate, however, because of the saturation of HR response to sympathetic nerve stimulation. The increase of RRI variation was not proportional to the increase in the stimulus rate either, suggesting that the saturation effect observed in the HR response was not an artifact of reciprocal relationship between RRI and HR.

Table 2. *Parameters of the transfer functions and step responses*

	Control	Yohimbine
K, beats·min^{-1}·Hz^{-1}	7.3±1.1	12.0±2.1*
f_N, Hz	0.081±0.012	0.055±0.008*
ζ	1.64±0.47	1.55±0.21
L, s	0.82±0.22	1.03±0.19
Fitting error, %	5.6±1.5	3.6±1.1
S, beats/min	7.2±0.8	12.2±1.7*
α, beats·min^{-1}·s^{-1}	0.93±0.23	0.94±0.22
S/α, s	9.1±1.4	14.4±1.9*

Values are means ± SE. K, steady-state gain; f_N, natural frequency; ζ, damping coefficient; L, pure dead time; S, steady-state response; α, initial slope; S/α, ratio of S to α. *$P < 0.05$ vs. control values.

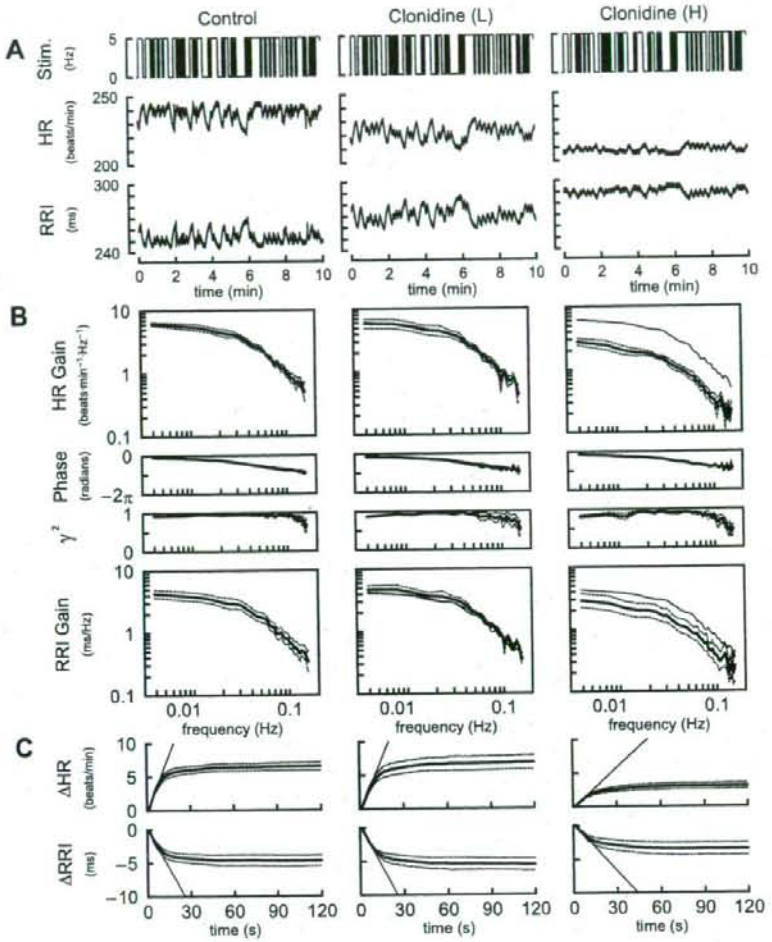

Fig. 3. *A:* representative recordings of cardiac sympathetic nerve stimulation rate (*top*), HR response (*middle*), and RRI response (*bottom*) under conditions of control (*left*), lower-dose clonidine (0.3 $mg \cdot kg^{-1} \cdot h^{-1}$; *middle*), and higher-dose clonidine (1.5 $mg \cdot kg^{-1} \cdot h^{-1}$; *right*) obtained in *protocol 2*. Clonidine activates the presynaptic α_2-adrenergic inhibition independent of the amount of norepinephrine released at the sympathetic nerve terminals. The amplitude of HR variation becomes smaller, and the mean level of HR becomes lower in the presence of higher-dose clonidine. The amplitude of RRI response also became smaller under higher-dose clonidine condition. *B:* transfer functions averaged over all animals in *protocol 2*. HR gain plots (*top*), phase plots (*second*), coherence functions (γ_2, *third*), and RRI gain plots (*bottom*). Lower-dose clonidine does not affect the transfer function significantly. Higher-dose clonidine decreases the dynamic gain in the whole frequency range (0.004 to 0.2 Hz). The fine solid curves in the gain plots (*middle* and *right*) duplicate the mean gain plot (*left*). *C:* step responses of HR (*top*) and RRI (*bottom*) calculated from the corresponding transfer functions. Lower-dose clonidine does not affect the step response significantly. Higher-dose clonidine attenuates the steady-state response accompanied by a decrease in the initial slope of the response (fine oblique line). Bold, solid lines represent the mean, whereas dotted lines indicate means ± SE.

Table 5 summarizes the mean HR and AP obtained from the supplemental protocol. There were no significant differences in mean HR and AP before cardiac sympathetic nerve stimulation. Mean HR was higher in $Bin_{0\text{-}3}$ and $Bin_{0\text{-}5}$ than in $Bin_{0\text{-}1}$ condition. Mean AP did not differ among the three conditions.

Figure 4*B* illustrates the transfer function averaged from the five animals in the supplemental protocol. The contour of HR gain plots showed an approximately downward shift with increase in the stimulus rate of the binary white noise signal, indicating that the augmentation of the HR variation seen in Fig. 4*A* was not proportional to the increase in the stimulus rate. No significant differences were noted in the phase plot. The coherence values were slightly decreased in all frequencies with increase in the stimulus rate of the binary white noise signal, suggesting that the HR response became saturated and the linearity between the stimulation and the HR response was

Table 3. *Mean heart rate and arterial pressure before and during random stimulation of the cardiac sympathetic nerve*

	Control	Clonidine (L)	Clonidine (H)
Heart rate, beats/min			
Before	277±16	250±15	232±20*
During	299±14	271±14	246±27*
Mean arterial pressure, mmHg			
Before	95±6	77±8	113±9
During	96±6	79±9	115±13

Values are means ± SE. Data were obtained after vagal and cardiac sympathetic nerves were cut. *$P < 0.05$ vs. control values by Dunnett's test.

Table 4. *Transfer function parameters and step responses*

	Control	Clonidine (L)	Clonidine (H)
K, $beats \cdot min^{-1} \cdot Hz^{-1}$	6.4±0.8	6.8±1.1	2.7±0.5*
f_N, Hz	0.066±0.017	0.070±0.016	0.059±0.013
ζ	1.56±0.37	1.72±0.23	1.55±0.20
L, s	0.56±0.17	1.24±0.20*	1.03±0.18
Fitting error, %	2.9±1.2	4.2±1.5	5.5±2.3
S, beats/min	6.3±0.8	6.8±1.0	2.8±0.5*
α, $beats \cdot min^{-1} \cdot s^{-1}$	0.56±0.07	0.51±0.04	0.22±0.06*
S/α, s	11.2±0.7	13.1±1.3	13.8±1.2

Values are means ± SE. *$P < 0.05$ vs. control values.

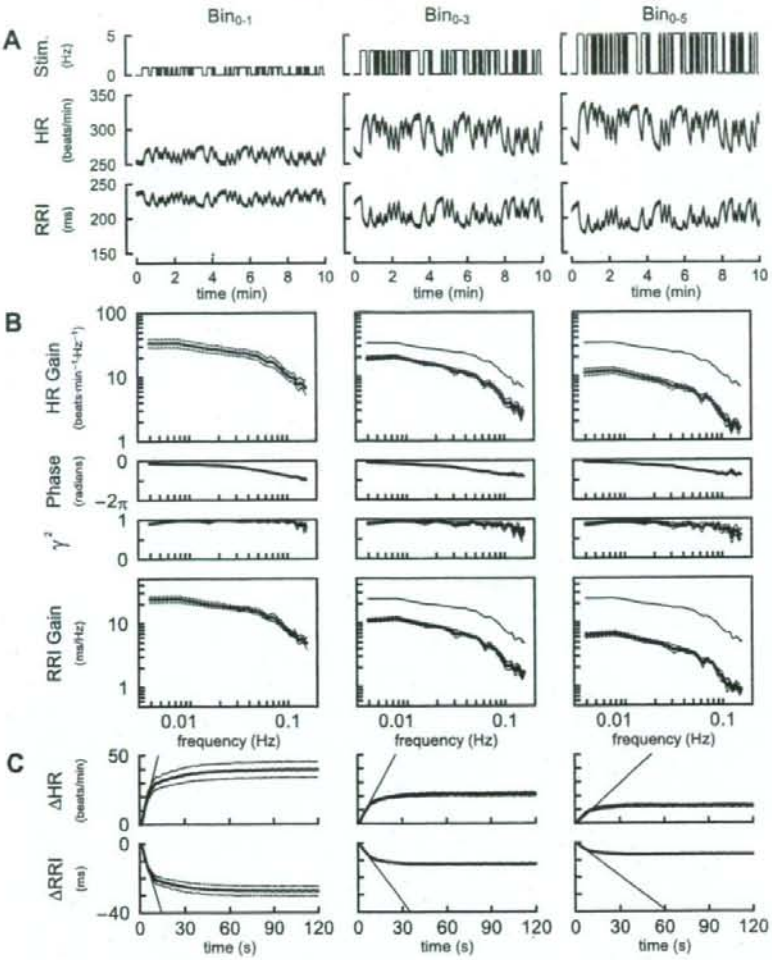

Fig. 4. *A*: representative recordings of cardiac sympathetic nerve stimulation rate (*top*), HR response (*middle*), and RRI response (*bottom*) obtained by differing the stimulus rate of the binary white noise signal. Bin_{0-1}, binary white noise between 0 and 1 Hz; Bin_{0-3}, binary white noise between 0 and 3 Hz; Bin_{0-5}, binary white noise between 0 and 5 Hz. Increasing the stimulus rate of the binary white noise signal augments the magnitude of HR response and increased mean HR. The RRI response was also increased with increasing the stimulus rate. *B*: transfer functions averaged over all animals in the supplemental protocol. HR gain plots (*top*), phase plots (*second*), coherence functions (γ_2, *third*), and RRI gain plots (*bottom*). Increasing the stimulus rate of the binary white noise signal decreases the dynamic gain in the whole frequency range (0.004 to 0.2 Hz). The fine solid curves in the gain plots (*middle* and *right*) duplicate the mean gain plot (*left*). *C*: step responses of HR (*top*) and RRI (*bottom*) calculated from the transfer functions. Increasing the stimulus rate of the binary white noise signal attenuates the steady-state response accompanied by a decrease in the initial slope of the response (fine oblique line). Bold, solid lines represent the mean, whereas dotted lines indicate means ± SE.

slightly reduced in Bin_{0-3} and Bin_{0-5} compared with that in Bin_{0-1} condition. The contour of RRI gain plots also showed approximately downward shift with increasing the stimulus rate of the binary white noise signal.

Figure 4*C* represents the step response of HR to sympathetic nerve stimulation calculated from the transfer functions shown in Fig. 4*B*. The increase in the stimulus rate of the binary white noise signal attenuated the steady-state response and also reduced the initial slope of the response. In the RRI step

Table 5. *Mean heart rate and arterial pressure before and during random stimulation of the cardiac sympathetic nerve*

	Bin_{0-1}	Bin_{0-3}	Bin_{0-5}
Heart rate, beats/min			
Before	268±6	269±7	266±5
During	292±8	330±9*	341±11*
Mean arterial pressure, mmHg			
Before	84±7	82±5	88±12
During	94±7	94±7	95±9

Values are means ± SE. Data were obtained after vagal and cardiac sympathetic nerves were cut. Bin_{0-1}, Bin_{0-3}, and Bin_{0-5}: binary white noise signals of 0–1, 0–3, and 0–5 Hz, respectively. *$P < 0.01$ vs. Bin_{0-1} values by Tukey test. There were no significant differences in parameters between Bin_{0-3} and Bin_{0-5}.

Table 6. *Transfer function parameters and step responses*

	Bin_{0-1}	Bin_{0-3}	Bin_{0-5}
K, beats·min^{-1}·Hz^{-1}	36.2±4.9	20.0±1.1†	11.8±1.1†
f_N, Hz	0.098±0.009	0.079±0.006*	0.078±0.006*
Z	1.56±0.04	1.68±0.04*	1.68±0.05*
L, s	0.95±0.01	0.97±0.01	0.97±0.01
Fitting error, %	4.8±1.1	3.2±0.8	3.5±0.5
S, beats/min	40.9±5.1	22.1±1.6†	12.8±1.4†
α, beats·min^{-1}·s^{-1}	4.23±0.61	2.00±0.21†	1.20±0.17†
S/α, s	9.9±0.5	11.3±0.8	10.8±0.8

Values are means ± SE. †$P < 0.01$ and *$P < 0.05$ vs. Bin_{0-1} values by Tukey test. There were no significant differences in parameters between Bin_{0-3} and Bin_{0-5}.

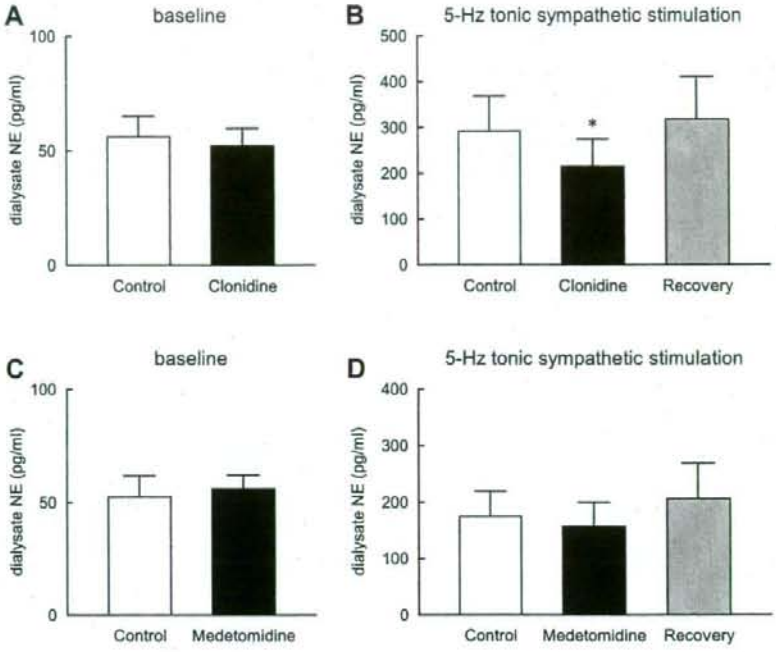

Fig. 5. Effects of clonidine (1.5 mg·kg^{-1}·h^{-1} iv) or medetomidine (1.5 mg·kg^{-1}·h^{-1} iv) on the myocardial interstitial norepinephrine (NE) release in response to 5-Hz tonic cardiac sympathetic nerve stimulation. Data were obtained after sectioning vagal and cardiac sympathetic nerves. Clonidine administration does not affect baseline levels of NE (*A*), but significantly attenuates the stimulation-induced NE release (*B*). *C*: medetomidine administration does not affect baseline levels of NE. *D*: it does not attenuate the stimulation-induced NE release significantly. Values are means ± SE. *$P < 0.05$ from control.

response, the steady-state response was attenuated from -27.6 ± 2.8 to -12.2 ± 0.7 ($P < 0.01$) and -6.7 ± 0.4 ($P < 0.01$) ms during Bin_{0-3} and Bin_{0-5}, respectively. The initial slope was attenuated from -3.0 ± 0.3 to -1.1 ± 0.1 ($P < 0.01$) and -0.65 ± 0.06 ($P < 0.01$) ms/s during Bin_{0-3} and Bin_{0-5}, respectively.

Parameters of the transfer functions and step responses estimated in the supplemental protocol are summarized in Table 6. The steady-state gain of the transfer function and the steady-state response of the corresponding step response decreased with increase in the stimulus rate of the binary white noise sequence. Although the initial slope of the step response significantly decreased with increase in the stimulus rate of the binary white noise signal, the ratio of the steady-state response to the initial slope was unchanged. The natural frequency was lower and the damping coefficient was greater in Bin_{0-3} and Bin_{0-5} than Bin_{0-1} condition. The pure dead time of the transfer function did not differ among the three conditions.

Figure 5 summarizes the results of the supplemental protocol of NE measurement. Baseline levels of myocardial interstitial NE did not differ before and during clonidine administration (Fig. 5*A*). Clonidine administration attenuated the sympathetic stimulation-induced NE release to 75.8 ± 5.4% of the control ($P < 0.05$) (Fig. 5*B*). Baseline NE levels did not differ before and during medetomidine administration (Fig. 5*C*). Medetomidine did not attenuate the sympathetic stimulation-induced NE release significantly (92.0 ± 6.7% of the control, not significant) (Fig. 5*D*).

Simulation Study

To explore possible mechanisms for the observed differences between the presynaptic α_2-adrenergic autoinhibition and the pharmacologic augmentation of the presynaptic inhibition via the α_2-adrenergic receptors, we performed a simulation on the negative feedback regulation of the HR response to the sympathetic nerve stimulation. With reference to Fig. 6*A*, H_{FW} and H_{FB} represent the transfer functions of the forward path and the feedback path, respectively. A step input signal represents the sympathetic nerve stimulation. Both signals from presynaptic α_2-adrenergic autoinhibition and pharmacologic augmentation of the presynaptic inhibition attenuate the input signal via the same α_2-adrenergic receptors. Because the amount of neurotransmitter release cannot become negative, a threshold operator (Th) is added. The threshold operator is described mathematically as follows.

$$\mathrm{Th}(x) = x \text{ when } x > 0, \text{ otherwise } \mathrm{Th}(x) = 0$$

The output from the threshold operator or the amount of neurotransmitter is then fed into H_{FW} to yield the output or change in HR and is also fed into H_{FB} to yield the feedback signal of presynaptic α_2-adrenergic autoinhibition. Since we administered clonidine ~15 min before sympathetic nerve stimulation, the effect of clonidine should have reached the steady state at the time of sympathetic nerve stimulation. Accordingly, we treated the pharmacologic augmentation of the presynaptic inhibition as a constant input. The magnitude of pharmacologic augmentation of the presynaptic inhibition was set arbitrarily to 0.5 to mimic the results of higher dose clonidine in *protocol 2*. The simulation was conducted using Matlab Simulink (The Mathworks, Natick, MA).

Yohimbine administration corresponds to severing the feedback path, i.e., setting $H_{FB} = 0$ in the simulation. Under this condition, the transfer function from the input to output becomes H_{FW}. Therefore, we modeled H_{FW} using the second-order, low-pass filter with pure dead time (*Eq. 3*) with the

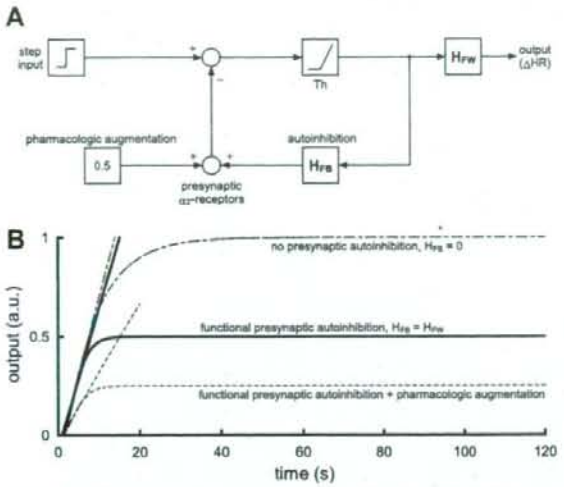

Fig. 6. Possible theoretical explanation for the differential effects of presynaptic α_2-adrenergic autoinhibition and pharmacologic augmentation of presynaptic α_2-adrenergic inhibition on the HR response to sympathetic nerve stimulation. *A:* a simulation model for the HR step response to a step input in the sympathetic nerve activity. H_{FW}, transfer function of the forward path; H_{FB}, transfer function of the feedback path; Th, a threshold operator (see main text for details). *B:* simulation results under conditions of no presynaptic inhibition (dash-dot line; H_{FB} = 0 and pharmacologic augmentation of presynaptic inhibition = 0, corresponding to the yohimbine administration condition), functional presynaptic α_2-adrenergic autoinhibition (solid line; H_{FB} = H_{FW} and pharmacologic augmentation of presynaptic inhibition = 0, corresponding to the control condition), and functional presynaptic α_2-adrenergic autoinhibition plus pharmacologic augmentation of the presynaptic inhibition (dotted line; H_{FB} = H_{FW} and pharmacologic augmentation of presynaptic inhibition = 0.5, corresponding to the higher-dose clonidine condition). The presynaptic α_2-adrenergic autoinhibition does not attenuate the initial slope of the step response. In contrast, the pharmacologic augmentation of the presynaptic inhibition attenuates the initial slope of the step response.

settings of f_N = 0.055, ζ = 1.55, and L = 0.94 (Table 2, yohinbine). The gain was set at unity for simplicity. With this setting, we calculated the output response to the unit step input without the presynaptic inhibition (Fig. 6*B*, dash-dot line, corresponding to the yohimbine condition). The initial slope of the response, calculated from the linear regression analysis described in the method section, was 0.0763 arbitrary units (AU)/s. Next, we set H_{FB} = H_{FW} and performed a simulation of the condition with the presynaptic α_2-adrenergic autoinhibition (Fig. 6*B*, solid line, corresponding to the control condition). The presynaptic α_2-adrenergic autoinhibition attenuates the steady-state response without significantly affecting the initial slope of the response (0.0695 AU/s). Finally, we set the pharmacologic augmentation of the presynaptic inhibition to 0.5 on top of the functioning H_{FB}. The simulation result (Fig. 6*B*, dotted line, corresponding to the higher dose clonidine condition) demonstrates that pharmacologic augmentation of the presynaptic inhibition attenuates the steady-state response accompanied by a reduction in the initial slope of the response (0.0346 AU/s).

DISCUSSION

We compared the blockade and activation of the presynaptic α_2-adrenergic receptors and found a difference between the presynaptic α_2-adrenergic autoinhibition and the pharmacologic augmentation of the presynaptic inhibition in terms of HR response to sympathetic nerve stimulation. The presynaptic α_2-adrenergic autoinhibition showed a limiter-like operation that restricts the steady-state response without affecting the initial slope of the response. In contrast, the pharmacologic augmentation of presynaptic inhibition showed an attenuator-like operation that reduces both the steady-state response and the initial slope of the response.

Comparison of Blocking and Activating the Presynaptic α_2-Adrenergic Receptors

Although the presynaptic α_2-adrenergic negative feedback has been known to attenuate the NE release and HR response to sympathetic nerve stimulation (9, 21, 26, 27, 29, 30, 31), the dynamic nature of the negative feedback remained to be elucidated. As shown in Fig. 2*C*, the blockade of α_2-adrenergic receptors by yohimbine increased the steady-state response without significantly affecting the initial slope of the HR step response (Table 2). That is to say, the presynaptic α_2-adrenergic autoinhibition of the presynaptic inhibition attenuates the steady-state response without sacrificing the rising speed of HR response to sympathetic nerve stimulation under control condition. These characteristics of the presynaptic α_2-adrenergic autoinhibition conform to the limiter-like operation shown in Fig. 1*A*. In contrast, pharmacologic augmentation of the presynaptic inhibition by higher dose clonidine reduced the steady-state response accompanied by a decrease in the initial slope of the HR step response (Fig. 3*C*). The ratio of the steady-state response to the initial slope was not changed significantly by higher dose clonidine (Table 4), suggesting that attenuation of the initial slope was proportional to that of the steady-state response. These characteristics of the pharmacologic augmentation of the presynaptic inhibition conform to the attenuator-like operation shown in Fig. 1*B*. Rapid effector response is one of the most important hallmarks of neural regulation compared with humoral regulation. The findings of the present study suggest that presynaptic α_2-adrenergic autoinhibition, but not pharmacologic augmentation of the presynaptic α_2-adrenergic inhibition, prevents excess NE outflow at the sympathetic nerve terminals without compromising the rapidity of effector response. The simulation results suggest that the initial slope of the response decreases when presynaptic inhibition occurs, independent of the negative feedback mechanism (Fig. 6*B*). On the other hand, the initial slope of the response does not decrease significantly when the presynaptic inhibition occurs through the negative feedback mechanism.

α_2-Adrenergic receptors are classified as α_{2A}-, α_{2B}-, and α_{2C}-subtypes based on gene encodings (26). Furthermore, the different ligand binding characteristics of the α_{2A}-subtype give rise to the pharmacological subtype of α_{2A} in humans, rabbits, and pigs and that of α_{2D} in rats, mice, and guinea pigs (26). The α_{2A} and α_{2D} may be considered as "orthologous" α_2-receptors, with only one being present in any given species (27). In the sympathetic nerve, α_{2A}- and α_{2C}-receptors operate as presynaptic inhibitory autoreceptors, whereas α_{2B}-receptors are located on postsynaptic cells to mediate the effects of catecholamine, such as vasoconstriction (26). In tissue slices from mouse atria, α_{2A}-receptors inhibit NE release from sympathetic nerves primarily at high-stimulation rates (1–2 Hz), whereas

α_{2C}-receptors can operate at very low stimulation rates (0.05–0.1 Hz) (10). Because α_2-receptors in the rabbit heart are characterized as α_{2A}, changes in the transfer function from sympathetic nerve stimulation to HR response observed in the present study are most likely mediated by α_{2A}-receptors.

Clonidine administration (5 μg/kg bolus followed by 30 $\mu g \cdot kg^{-1} \cdot h^{-1}$ iv) attenuated the sympathetic outflow from the central nervous system in rabbits (35). However, lower dose clonidine at 0.3 $mg \cdot kg^{-1} \cdot h^{-1}$ failed to significantly affect the steady-state response or the initial slope of the HR step response in the present study (Fig. 3*B*, Table 4), suggesting a difference in clonidine sensitivity between the central and peripheral sympathetic nervous systems. Another factor that should be taken into account is the operating range of the HR control (i.e., mean HR during dynamic sympathetic stimulation). As an example, tonic vagal stimulation decreased mean HR during dynamic sympathetic stimulation, which increased the dynamic gain of sympathetic HR control via nonlinear sigmoidal input-output nature between autonomic activities and HR (12, 13). Therefore, the decrease in the mean HR during lower dose clonidine, although it was statistically insignificant (Table 3), should have an effect of increasing the dynamic gain of the sympathetic HR control. Such an effect might have counterbalanced the effect of reducing the dynamic gain via presynaptic inhibition during the lower dose clonidine administration. Although higher dose clonidine decreased mean HR before and during sympathetic nerve stimulation, mean AP did not decrease compared with lower dose clonidine (Table 3). The discrepancy between the changes in mean HR and AP may be due to direct vasoconstriction by higher dose clonidine through α-adrenergic stimulation.

Transfer Function Analysis vs. Step Response Analysis

In a previous study, our laboratory performed a transfer function analysis on the sympathetic HR control using a binary white noise signal (12, 23). The transfer function is a frequency-domain representation of the system dynamic characteristics over a wide frequency range and is useful for understanding the behavior of the system in response to a variety of input signals (3, 7, 21). Notwithstanding the theoretical advantages of the transfer function, the frequency-domain representation may be somewhat unfamiliar to most physiologists. Therefore, we calculated the step responses corresponding to the transfer functions. As can be seen in Figs. 2, *B* and *C* and 3, *B* and *C*, changes in transfer function in the lower frequency range reflect the steady-state response in the step response. Changes in transfer function in the higher frequency reflect the initial transient response in the step response. Because the step response and the transfer function are mathematically interchangeable, both the transfer function and the step response provide comparable information on the system dynamic characteristics.

In a previous study, our laboratory has shown that increasing mean stimulus rate of the Gaussian white noise decreased the steady-state gain of the transfer function from sympathetic nerve stimulation to HR without affecting the natural frequency or damping coefficient significantly (23). Increasing the stimulus rate of the binary white noise signal also caused an approximately parallel downward shift in the gain plot (Fig. 4*B*). The transfer function parameters, however, showed a decrease in the natural frequency and an increase in the damping coefficient (Table 6). The higher natural frequency in $Bin_{0\text{-}1}$ than in $Bin_{0\text{-}5}$ condition may account for the higher natural frequency in *protocol 1* ($Bin_{0\text{-}1}$ was used for sympathetic stimulation) than in *protocol 2* ($Bin_{0\text{-}5}$ was used for sympathetic stimulation) observed under control conditions. Notwithstanding the differences in the natural frequency and the damping coefficient, the ratio of the step response to the initial slope was not changed significantly by the difference in the stimulus rate of the binary white noise signal. Therefore, yohimbine-induced changes in the ratio of the step response to the initial slope observed in *protocol 1* (Table 1) cannot be explained by changes in the magnitude of sympathetic effect on HR.

Limitations

The present study has several limitations. First, we performed the experiment under anesthetic conditions. However, because we compared the effects of yohimbine and clonidine on the sympathetic HR control under the same anesthetic

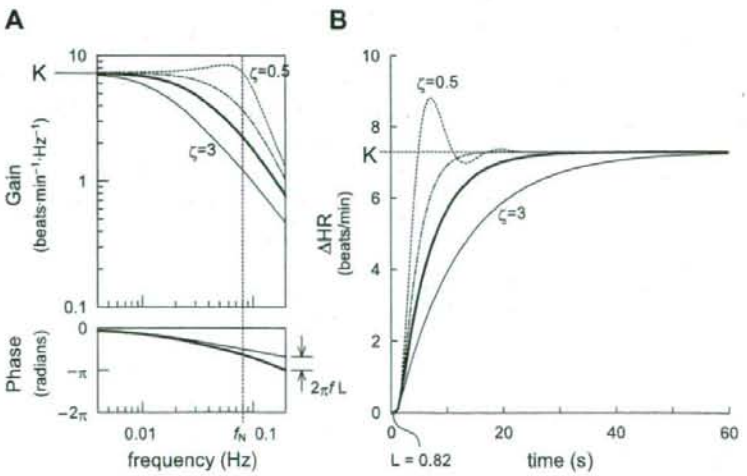

Fig. 7. Schematic explanation for the frequency response of a second-order, low-pass filter with pure dead time (*L*; *A*), and the corresponding step response (*B*). *K*, dynamic gain; f_N, natural frequency; ζ, damping ratio. See APPENDIX for details.

condition, the interpretation of the observed changes in the transfer function may be reasonable. Second, the simulation model in Fig. 6*A* is not the only model that can be applied to the observed results. Although the model is convenient to explain many aspects of the observed results, other models may also be applicable to the present observation. Third, clonidine can affect HR through non-α_2-adrenergic mechanisms. For instance, clonidine caused bradycardia in α_{2ABC}-knockout mouse via direct inhibition of cardiac hyperpolarization-activated cyclic nucleotide-gated pacemaker channels (16). While we tried to use medetomidine instead of clonidine, medetomidine did not attenuate myocardial interstitial NE release in response to sympathetic nerve stimulation significantly, at least, at the same dose as clonidine (Fig. 5). Further studies using other agonists might be required to confirm our observations. Finally, we used a weak stimulus rate (0 to 1 Hz) for the yohimbine protocol. Although we had examined the effect of yohimbine using a strong stimulus rate (0–5 Hz) in a preliminary study, the steady-state gain of the transfer function did not increase much (8.4 ± 1.7 vs. 9.0 ± 1.7 beats·min^{-1}·Hz^{-1}, $n = 3$). Under such strong stimulus condition, the saturation of HR response might have masked the effect of presynaptic inhibition. Therefore, the result of *protocol 1* should be carefully interpreted in view of the existence of a stimulus rate-drug interaction effect.

Conclusions

The presynaptic α_2-adrenergic autoinhibition attenuates the dynamic HR response to sympathetic nerve stimulation in the low-frequency range (0.004–0.04 Hz) but not in the high-frequency range (0.05–0.15 Hz). In the time domain, the presynaptic α_2-adrenergic autoinhibition attenuates the steady-state response without affecting the slope of the response in the HR step response (a limiter-like operation). In contrast, pharmacologic augmentation of presynaptic α_2-adrenergic inhibition attenuates the dynamic HR response to sympathetic nerve stimulation in a frequency-independent manner. In the time domain, pharmacologic augmentation of the presynaptic inhibition attenuates not only the steady-state response but also the initial slope of the HR step response (an attenuator-like operation). Presynaptic α_2-adrenergic autoinhibition would be favorable for limiting excess NE outflow at the sympathetic nerve terminals without compromising the rapidity of effector response.

APPENDIX

Mathematical Modeling of the Sympathetic HR Response

To describe the estimated transfer function, we used a second-order, low-pass filter with pure dead time (L). Figure 7*A* shows the frequency response of a second-order, low-pass filter with L. Figure 7*B* shows the corresponding step response. The step response is calculated for 1-Hz sympathetic nerve stimulation. The steady-state gain (K) of the transfer function represents the value of transfer gain as the frequency approaches zero. The K corresponds to the steady-state response in the step-response representation. The natural frequency (f_N) determines the upper frequency limit of the low-pass filter. For instance, if the f_N were 10 times higher, the frequency axis in Fig. 7*A* would have to be scaled by a factor of 10, indicating that the system could respond to 10-fold higher frequency input. The phase plot in Fig. 7*A* indicates that, at the f_N, the output is delayed by $\pi/2$ radians relative to the input, in the absence of the L. The maximum phase delay of the second-order, low-pass filter is π radians in the absence of L. The L is needed to account for the phase difference between the estimated transfer function and the second-order, low-pass filter. In Fig. 7*B*, the L corresponds to the time difference between the onset of the step input and the onset of the response. The damping coefficient (ζ) characterizes the system response around the f_N. As an example, the gain plot shows a slight peak around f_N when $\zeta = 0.5$ (dotted line). Figure 7*B* shows that a ζ of 0.5 causes an initial overshoot in response to a step change in the input. A system with $\zeta < 1$ is called underdamped. On the other hand, the gain plot shows more gradual decrease around f_N when $\zeta = 3$ (fine solid line). Figure 7*B* shows that the system responds sluggishly when $\zeta = 3$. A system with $\zeta > 1$ is called overdamped. A system with $\zeta = 1$ is called critically damped (dash-dot line). The ζ of the estimated transfer functions ranged from 1.55 to 1.72 in the present study, indicating that the sympathetic HR control system is overdamped. The solid line represents the second-order, low-pass filter with $\zeta = 1.64$ and $L = 0.82$ that is derived from the mean value obtained under control condition in *protocol 1*.

GRANTS

This study was supported by "Health and Labour Sciences Research Grant for Research on Advanced Medical Technology," "Health and Labour Sciences Research Grant for Research on Medical Devices for Analyzing, Supporting and Substituting the Function of Human Body," and "Health and Labour Sciences Research Grant H18-Iryo-Ippan-023" from the Ministry of Health, Labour and Welfare of Japan; "Program for Promotion of Fundamental Studies in Health Science" from the National Institute of Biomedical Innovation; and "Ground-based Research Announcement for Space Utilization" promoted by the Japan Space Forum.

REFERENCES

1. **Altman JD, Trendelenburg AU, MacMillan L, Bernstein D, Limbird L, Starke K, Kobilka BK, Hein L.** Abnormal regulation of the sympathetic nervous system in α_{2A}-adrenergic receptor knockout mice. *Mol Pharmacol* 56: 154–161, 1999.
2. **Bendat JS, Piersol AG.** Single-input/output relationships. In: *Random Data Analysis and Measurement Procedures* (3rd Ed.). New York: Wiley, 2000, p. 189–217.
3. **Berger RD, Saul JP, Cohen RJ.** Transfer function analysis of autonomic regulation. I. Canine atrial rate response. *Am J Physiol Heart Circ Physiol* 256: H142–H152, 1989.
5. **Brigham EO.** FFT transform applications. In: *The Fast Fourier Transform and Its Applications*. Englewood Cliffs, NJ: Prentice-Hall, 1988, p. 167–203.
6. **Buhler FR, Bolli P, Amann WF, Erne P, Kiowski W.** Sympathetic nervous system in essential hypertension and antihypertensive response to α_2-adrenoceptor stimulation. *J Cardiovasc Pharmacol* 6: S753–S756, 1984.
7. **Franklin GF, Powell JD, and Emani-Naeini A.** Dynamic models and dynamic response. In: *Feedback Control of Dynamic Systems* (2nd Ed.). Boston, MA: Addison-Wesley, 1991, p. 17–144.
8. **Glantz SA.** *Primer of Biostatistics* (5th Ed.). New York: McGraw-Hill, 2002.
9. **Grossman E, Chang PC, Hoffman A, Tamrat M, Goldstein DS.** Evidence for functional α_2-adrenoceptors on vascular sympathetic nerve endings in the human forearm. *Circ Res* 69: 887–897, 1991.
10. **Hein L, Altman JD, Kobilka BK.** Two functionally distinct α2-adrenergic receptors regulate sympathetic neurotransmission. *Nature* 402: 181–184, 1999.
11. **Jie K, van Brummelen P, Vermey P, Timmermans PB, van Zwieten PA.** Modulation of noradrenaline release by peripheral presynaptic α_2-adrenoceptors in humans. *J Cardiovasc Pharmacol* 9: 407–413, 1987.
12. **Kawada T, Ikeda Y, Sugimachi M, Shishido T, Kawaguchi O, Yamazaki T, Alexander J Jr, Sunagawa K.** Bidirectional augmentation of heart rate regulation by autonomic nervous system in rabbits. *Am J Physiol Heart Circ Physiol* 271: H288–H295, 1996.
13. **Kawada T, Sugimachi M, Shishido T, Miyano H, Sato T, Yoshimura R, Miyashita H, Nakahara T, Alexander J Jr, Sunagawa K.** Simultaneous identification of static and dynamic vagosympathetic interactions in regulating heart rate. *Am J Physiol Regul Integr Comp Physiol* 276: R782–R789, 1999.

14. **Kawada T, Yamazaki T, Akiyama T, Sato T, Shishido T, Sugimachi M, Inagaki M, Alexander J Jr, Sunagawa K.** Liquid chromatographic determination of myocardial interstitial epinephrine. *J Chromatogr B Biomed Sci Appl* 714: 375–378, 1998.
15. **Kawada T, Yamazaki T, Akiyama T, Sato T, Shishido T, Yoshimura R, Inagaki M, Tatewaki T, Sugimachi M, Sunagawa K.** Local epinephrine release in the rabbit myocardial interstitium in vivo. *J Auton Nerv Syst* 78: 94–98, 2000.
16. **Knaus A, Zong X, Beetz N, Jahns R, Lohse MJ, Biel M, Hein L.** Direct inhibition of cardiac hyperpolarization-activated cyclic nucleotide-gated pacemaker channels by clonidine. *Circulation* 115: 872–880, 2007.
17. **Langer SZ.** 25 years since the discovery of presynaptic receptors, present knowledge and future perspectives. *Trends Pharmacol Sci* 18: 95–99, 1997.
18. **Langer SZ.** Presence and physiological role of presynaptic inhibitory α_2-adrenoreceptors in guinea pig atria. *Nature* 294: 671–672, 1981.
19. **Langer SZ, Adler-Graschinsky E, Giorgi O.** Physiological significance of α-adrenoceptor-mediated negative feedback mechanism regulating noradrenaline release during nerve stimulation. *Nature* 265: 648–650, 1977.
20. **Langer SZ.** Presynaptic regulation of catecholamine release. *Biochem Pharmacol* 23: 1793–1800, 1974.
21. **Marmarelis PZ, Marmarelis VZ.** The white noise method in system identification. In: *Analysis of Physiological Systems*. New York: Plenum, 1978, p. 131–221.
22. **Miyamoto T, Kawada T, Yanagiya Y, Takaki H, Inagaki M, Sugimachi M, Sunagawa K.** Cardiac sympathetic nerve stimulation does not attenuate dynamic vagal control of heart rate via α-adrenergic mechanism. *Am J Physiol Heart Circ Physiol* 287: H860–H865, 2004.
23. **Nakahara T, Kawada T, Sugimachi M, Miyano H, Sato T, Shishido T, Yoshimura R, Miyashita H, Inagaki M, Alexander J Jr, Sunagawa K.** Neuronal uptake affects dynamic characteristics of heart rate response to sympathetic stimulation. *Am J Physiol Regul Integr Comp Physiol* 277: R140–R146, 1999.
24. **Niederhoffer N, Hein L, Starke K.** Modulation of the baroreceptor reflex by α_{2A}-adrenoceptors, a study in α_{2A} knockout mice. *Br J Pharmacol* 141: 851–859, 2004.
25. **Pelayo F, Dubocovich ML, Langer SZ.** Regulation of noradrenaline release in the rat pineal through a negative feedback mechanism mediated by presynaptic α-adrenoceptors. *Eur J Pharmacol* 45: 317–318, 1977.
26. **Philipp M, Brede M, Hein L.** Physiological significance of α_2-adrenergic receptor subtype diversity, one receptor is not enough. *Am J Physiol Regul Integr Comp Physiol* 283: R287–R295, 2002.
27. **Rump LC, Bohmann C, Schaible U, Schöllhorn J, Limberger N.** α2C-Adrenoceptor-modulated release of noradrenaline in human right atrium. *Br J Pharmacol* 116: 2617–2624, 1995.
27a. **Schwartz DD.** Activation of alpha-2 adrenergic receptors inhibits norepinephrine release by a pertussis toxin-insensitive pathway independent of changes in cytosolic calcium in cultured rat sympathetic neurons. *J Pharmacol Exp Ther* 282: 248–255, 1997.
28. **Sinclair MD.** A review of the physiological effects of α2-agonists related to the clinical use of medetomidine in small animal practice. *Can Vet J* 44: 885–897, 2003.
29. **Starke KM, Gothert M, Kilbinger H.** Modulation of neurotransmitter release by presynaptic autoreceptors. *Physiol Rev* 69: 864–989, 1989.
30. **Starke KM.** Presynaptic α-autoreceptors. *Rev Physiol Biochem Pharmacol* 107: 73–146, 1987.
31. **Starke K, Langer SZ.** A note on terminology for presynaptic receptors. In: *Presynaptic Receptors*, edited by Langer SZ, Starke K, and Dubocovich ML. Oxford, UK: Pergamon 1979, p. 1–3.
32. **Starke K, Endo T, Taube HD.** Pre- and post-synaptic components in effect of drugs with α-adrenoceptor affinity. *Nature* 254: 440–441, 1975.
33. **Starke K.** Alpha sympathomimetic inhibition of adrenergic and cholinergic transmission in the rabbit heart. *Naunyn Schmiedebergs Arch Pharmacol* 274: 18–45, 1972.
34. **Szabo B, Schramm A, Starke K.** Effect of yohimbine on renal sympathetic nerve activity and renal norepinephrine spillover in anesthetized rabbits. *J Pharmacol Exp Ther* 260: 780–788, 1992.
35. **Szabo B, Hedler L, Starke K.** Peripheral presynaptic and central effects of clonidine, yohimbine and rauwolscine on the sympathetic nervous system in rabbits. *Naunyn-Schmiedeberg's Arch Pharmacol* 340: 648–657, 1989.
37. **Vizi ES, Somogyi GT, Hadhazy P, Knoll J.** Effect of duration and frequency of stimulation on the presynaptic inhibition by α-adrenoceptor stimulation of the adrenergic transmission. *Naunyn-Schmiedeberg's Arch Pharmacol* 280: 79–91, 1973.
38. **Westfall TC.** Local regulation of adrenergic neurotransmission. *Physiol Rev* 57: 659–728, 1977.

Life Sciences 83 (2008) 490–495

Contents lists available at ScienceDirect

Life Sciences

journal homepage: www.elsevier.com/locate/lifescie

Vagal stimulation suppresses ischemia-induced myocardial interstitial myoglobin release

Toru Kawada [a,*], Toji Yamazaki [b], Tsuyoshi Akiyama [b], Hirotoshi Kitagawa [c], Shuji Shimizu [a], Masaki Mizuno [a], Meihua Li [a], Masaru Sugimachi [a]

[a] Department of Cardiovascular Dynamics, Advanced Medical Engineering Center, National Cardiovascular Center Research Institute, Osaka 565-8565, Japan
[b] Department of Cardiac Physiology, National Cardiovascular Center Research Institute, Osaka 565-8565, Japan
[c] Department of Anesthesiology, Shiga University of Medical Science, Shiga 520-2192, Japan

ARTICLE INFO

Article history:
Received 19 May 2008
Accepted 23 July 2008

Keywords:
Coronary artery occlusion
Cardiac microdialysis
Cats

ABSTRACT

Aims: To evaluate vagal stimulation-mediated myocardial protection against ischemia and reperfusion in in vivo ischemic myocardium.
Main methods: We measured myocardial interstitial myoglobin levels in the ischemic region using a cardiac microdialysis technique in anesthetized and vagotomized cats. We occluded the left anterior descending coronary artery (LAD) for 60 min and reperfused it for 60 min (VX group, $n=6$). The effects of bilateral vagal stimulation (10 V, 5 Hz, 1-ms pulse duration), initiated immediately after LAD occlusion, were examined (VS group, $n=6$). To examine the involvement of phosphatidylinositol 3-kinase (PI3K), vagal stimulation was performed after pretreatment with a PI3K inhibitor wortmannin (0.6 mg/kg, i.v.) (VS-W group, $n=6$). To examine the contribution of bradycardia, vagal stimulation was performed with fixed-rate ventricular pacing (VS-P group, $n=6$).
Key findings: The average myoglobin level during the ischemic period was 1170±141 in VX (in ng/ml, mean±SE), which was significantly attenuated in VS (466±87, $P<0.05$) and VS-W (613±124, $P<0.05$) but not in VS-P (953±203). Reperfusion increased the myoglobin level to 2500±544 in VX, whereas it was suppressed in VS (824±213, $P<0.05$) and VS-W (948±315, $P<0.05$) but not in VS-P (1710±253).
Significance: Vagal stimulation, initiated immediately after LAD occlusion, attenuated the myocardial injury. Moreover, bradycardia, independent of PI3K pathway, plays a significant role in vagally induced cardioprotection during acute myocardial ischemia.

Introduction

An increase in parasympathetic tone can provide cardioprotection against acute myocardial ischemia and infarction via the direct effects of acetylcholine (ACh) on the ischemic myocardium and the indirect effects mediated by altered hemodynamics. For the direct effects, administration of ACh prior to a coronary artery occlusion reduces the infarct size in isolated, perfused rabbit heart (Qin et al., 2003). Phosphatidylinositol 3-kinase (PI3K) is thought to be an upstream enzyme in the signal transduction pathway for the ACh-induced, ischemic preconditioning mimetic effect (Qin et al., 2003; Oldenburg et al., 2003). For the indirect effects, vagal stimulation reduces myocardial oxygen consumption due to bradycardia (Sammel et al., 1983) and also decreases ventricular contractility via antagonism of the sympathetic effect (Nakayama et al., 2001). Vagal stimulation can also dilate the coronary artery (Feigl, 1969; Reid et al., 1985; Feliciano and Henning, 1998; Henning and Sawmiller, 2001), which may increase collateral flow into the ischemic region.

In a previous study, we demonstrated that efferent vagal stimulation nearly halved the increase in myocardial interstitial norepinephrine levels in the ischemic region of the feline ventricle (Kawada et al., 2006). Whether vagal stimulation can reduce myocardial damage in the ischemic region, however, has yet to be directly examined. To test the hypothesis that vagal stimulation reduces myocardial injury in the ischemic region, we measured myocardial interstitial myoglobin levels during acute myocardial ischemia and reperfusion with or without efferent vagal stimulation in anesthetized cats. We examined possible involvement of the PI3K signaling pathway using vagal stimulation and pretreatment with a PI3K inhibitor wortmannin. We also examined the contribution of bradycardia using vagal stimulation and fixed-rate ventricular pacing.

Materials and methods

Surgical preparation

Animal care was provided in strict accordance with the *Guiding Principles for the Care and Use of Animals in the Field of Physiological Sciences* approved by the Physiological Society of Japan. Adult cats

* Corresponding author. Department of Cardiovascular Dynamics, National Cardiovascular Center Research Institute, 5-7-1 Fujishirodai, Suita, Osaka 565-8565, Japan. Tel.: +81 6 6833 5012x2427; fax: +81 6 6835 5403.
E-mail address: torukawa@res.ncvc.go.jp (T. Kawada).

0024-3205/$ – see front matter © 2008 Elsevier Inc. All rights reserved.
doi:10.1016/j.lfs.2008.07.013

weighing between 2.3 and 4.2 kg were anesthetized with an intraperitoneal injection of pentobarbital sodium (30–35 mg/kg) and ventilated mechanically with room air mixed with oxygen. The depth of anesthesia was maintained with a continuous intravenous infusion of pentobarbital sodium (1–2 mg kg^{-1} h^{-1}) through a catheter inserted into the right femoral vein. Systemic arterial pressure (AP) was monitored from a catheter inserted into the right femoral artery. The heart rate (HR) was determined from an electrocardiogram using a cardiotachometer. The esophageal temperature of the animal was measured using a thermometer (CTM-303, TERUMO, Japan) and was maintained at approximately 37 °C using a heated pad and a lamp.

Bilateral vagal nerves were exposed and sectioned through a midline cervical incision. With the animal in the lateral position, the left fifth and sixth ribs were resected to allow access to the heart. The heart was suspended in a pericardial cradle. Using a fine guiding needle, a dialysis probe was implanted into the anterolateral free wall of the left ventricle perfused by the left anterior descending coronary artery (LAD) (Akiyama et al., 1994). A 3-0 silk suture was passed around the LAD just distal to the first diagonal branch for subsequent coronary occlusion. For bilateral vagal stimulation, a pair of bipolar platinum electrodes was attached to the cardiac end of each sectioned vagal nerve. The nerves and electrodes were covered with warmed mineral oil for insulation. Heparin sodium (100 U/kg) was administered intravenously to prevent blood coagulation. At the end of the experiment, the animals were killed with an overdose of intravenous pentobarbital sodium. We confirmed that the semipermeable membrane of the dialysis probe had been implanted within the left ventricular myocardium.

Dialysis technique

The materials and properties of the transverse dialysis probe have been previously described (Kitagawa et al., 2005). Briefly, both ends of a dialysis fiber (length, 8 mm; outer diameter, 215 μm; inner diameter, 175 μm; pore size, 300 Å; Evaflux type 5A, Kuraray Medical, Japan) were glued to polyethylene tubes (length, 25 cm; outer diameter, 500 μm; inner diameter, 200 μm). The dialysis probe was perfused with Ringer's solution at the rate of 5 μl/min using a microinfusion pump (CMA/100, Carnegie Medicine). Dialysate sampling was initiated 2 h after implanting the dialysis probe, at which point the concentration of myoglobin in the dialysate had reached a steady state (Kitagawa et al., 2005). The actual dialysate sampling period lagged behind a given collection period by 2 min due to the dead space volume between the dialysis membrane and the sample tube. The concentration of myoglobin in the dialysate was measured immunochemically (Cardiac Reader, Roche Diagnostics). The detection limit for myoglobin was 30 ng/ml. The sample was diluted in Ringer's solution whenever necessary and the concentration was corrected for the dilution factor.

Protocols

Protocol 1 (VX group, n=6)

As a control group, we measured changes in the myocardial interstitial myoglobin levels of vagotomized cats subjected to 60 min of LAD occlusion followed by 60 min of reperfusion. After collecting a 15-min baseline dialysate sample, we occluded the LAD for 60 min and collected four consecutive 15-min dialysate samples during the ischemic period. We then released the occlusion and collected additional four consecutive 15-min dialysate samples during the 60-min reperfusion period.

Protocol 2 (VS group, n=6)

We examined the effects of bilateral vagal stimulation on the release of myocardial interstitial myoglobin. To avoid the potential preconditioning mimetic effects of ACh released in response to the vagal stimulation (Kawada et al., 2002; Przyklenk and Kloner, 1995), we initiated bilateral vagal stimulation (5 Hz, 10 V, 1-ms pulse duration) immediately after the LAD occlusion and continued it throughout the 60-min ischemic period and the 60-min reperfusion period. Dialysate samples were collected in the same manner described for Protocol 1.

Protocol 3 (VS-W group, n=6)

Because PI3K is involved in the direct cardioprotective effects of ACh (Qin et al., 2003; Oldenburg et al., 2003), we examined the contribution of PI3K to the effects of vagal stimulation on ischemia-induced myocardial injury. A PI3K inhibitor wortmannin was administered (0.6 mg/kg i.v. bolus) 15 min before the onset of the baseline dialysate sampling. After collecting the baseline dialysate sample, LAD occlusion and reperfusion were each performed for 60 min. Bilateral vagal stimulation was started immediately after the LAD occlusion and was continued until the end of the reperfusion period. Dialysate samples were collected as described in Protocol 1.

Protocol 4 (VS-P group, n=6)

Because bradycardia is a major hemodynamic change induced by vagal stimulation, we examined the contribution of bradycardia to the effects of vagal stimulation on ischemia-induced myocardial injury. After collecting the baseline dialysate sample, LAD occlusion and reperfusion were each performed for 60 min. Bilateral vagal stimulation and fixed-rate ventricular pacing (200 beats/min) were both started immediately after the LAD occlusion and were continued throughout the ischemic and reperfusion periods. Dialysate samples were collected as described in Protocol 1.

Statistical analysis

All data are presented as the means and SE. To examine the effects of coronary occlusion and reperfusion on the myocardial interstitial myoglobin levels in each group, we compared the myoglobin levels during the ischemic and reperfusion periods with the baseline level (eight comparisons) and the myoglobin levels during the reperfusion period with the myoglobin level during the last 15 min of ischemia (four comparisons) using Holm's t test for 12 comparisons (Glantz, 2002). Briefly, after calculating P values for the 12 comparisons using paired-t test, the P values were sorted based on their size. The smallest P value was multiplied by 12 (the number of total comparisons), the next smallest P value was multiplied by 11 (the number of total comparisons minus 1), and so on. The Holm's test is less conservative than the ordinary Bonferroni method. Because the myoglobin level changed by more than an order of magnitude, comparisons were made after a logarithmic conversion. Differences were considered significant at $P<0.05$.

To compare myoglobin levels among the VX, VS, VS-W and VS-P groups, we used one-way ANOVA (analysis of variance). When there were significant differences among the groups, Dunnett's test was applied to examine the differences between the VS, VS-W, or VS-P group and the VX group (Glantz, 2002). The myoglobin levels at different time points as well as averaged myoglobin levels during the ischemic period, reperfusion period, and total period throughout ischemia and reperfusion were compared. Differences were considered significant at $P<0.05$.

HR and mean AP were measured immediately before the LAD occlusion (denoted as time 0), at 15, 30, 45 and 60 min of ischemia and at 15, 30, 45 and 60 min of reperfusion. The data for the HR and mean AP were compared among the VX, VS, VS-W, and VS-P groups using one-way ANOVA followed by Dunnett's test with the VX group value as the control. Differences were considered significant at $P<0.05$.

Results

Changes in the myocardial interstitial myoglobin levels are summarized in Fig. 1. In the VX group, the LAD occlusion significantly

increased the myoglobin levels compared with the baseline level, suggesting that acute myocardial ischemia disrupted the plasma membrane of the myocardium, allowing myoglobin to leak into the myocardial interstitium. The myoglobin level during the last 15 min of ischemia reached, on average, 12 times the baseline myoglobin level. Reperfusion further increased the myoglobin level. The myoglobin level during the first 15 min of reperfusion was, on average, three times higher than the myoglobin level during the last 15 min of ischemia. After 15 min of reperfusion, the myoglobin level declined gradually with time but remained higher than the baseline level until the last 15 min of the reperfusion period. In the VS group, the time course was similar but the changes in the myoglobin levels during the ischemia and reperfusion periods were smaller than those observed in the VX group. In the VS-W group, changes in the myoglobin levels were attenuated compared to those observed in the VX group and no significant increase in myoglobin was detected upon reperfusion. In the VS-P group, changes in the myoglobin levels showed intermediate values, which were between those observed in the VX and VS groups.

Baseline myoglobin levels were not significantly different among the VX, VS, VS-W, and VS-P groups (157±40, 110±23, 124±48, and 118±30 ng/ml, respectively). Average myoglobin levels for the ischemic period (Fig. 2A), reperfusion period (Fig. 2B), and total period (Fig. 2C) were significantly lower in the VS and VS-W groups compared with the VX group.

Changes in HR are summarized in the top panel of Fig. 3. Baseline HR did not markedly differ among the four groups. In the VS group (filled circles), vagal stimulation decreased the HR throughout the ischemic and reperfusion periods compared with the HR in the VX group (open circles). After the cessation of vagal stimulation (denoted as "vagal stim off"), the HR in the VS group returned toward the baseline level. In the VS-W group (double circles), vagal stimulation decreased the HR at 15 and 30 min compared with the results from the VX group. Although the HR from 45 to 120 min did not differ significantly compared with the VX group, the cessation of vagal stimulation increased the HR, suggesting that vagal stimulation was effective until the end of the reperfusion period. In the VS-P group (open squares), the HR was maintained at 200 beats/min using ventricular pacing. The cessation of ventricular pacing (denoted as "pacing off") significantly decreased the HR below the baseline level, suggesting that vagal stimulation was effective during the ventricular pacing.

Changes in AP are summarized in the bottom panel of Fig. 3. Differences in AP between the VS and VX groups were not statistically significant. Although pretreatment with wortmannin increased the AP in the VS-W group, differences in AP between the VS-W and VX groups were not statistically significant at any time point. In the VS-P group, AP at 15 min was significantly lower compared with that in the VX group.

Discussion

Vagal stimulation-induced cardioprotection against ischemic injury

Cardiac microdialysis is a useful method to monitor changes in myocardial interstitial myoglobin levels in an ischemic region (Kitagawa et al., 2005). LAD occlusion increased the myoglobin level in the myocardial interstitium in the VX group (Fig. 1). Vagal stimulation, initiated immediately after the LAD occlusion, suppressed myoglobin release during ischemia (Figs. 1 and 2A). In addition to preventing lethal ventricular arrhythmia during acute myocardial ischemia (Myers et al., 1974; Rosenshtraukh et al., 1994; Vanoli et al., 1991), vagal stimulation also appears to reduce myocardial damage in the ischemic region. Because we avoided large ischemia by occluding LAD just distal to the first diagonal branch, lethal ventricular

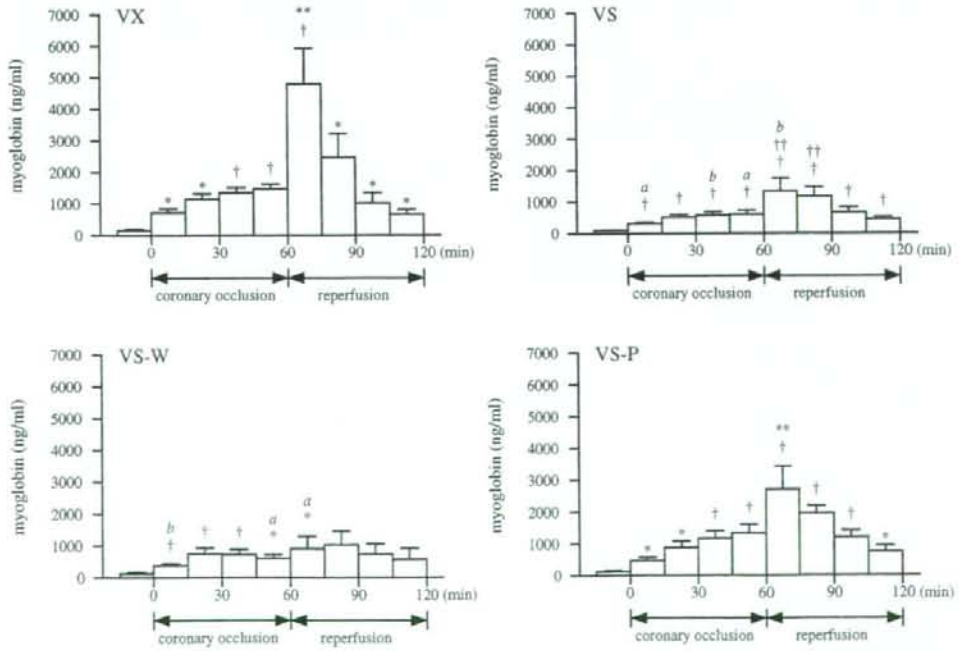

Fig. 1. Changes in the myocardial interstitial myoglobin levels in the VX, VS, VS-W, and VS-P groups. After collecting baseline dialysate samples, the left anterior descending coronary artery was occluded for 60 min and then reperfused for 60 min. Acute myocardial ischemia significantly increased the myoglobin level in the ischemic region. Reperfusion further increased the myoglobin level. Data are shown as the means+SE (n=6 each). †P<0.01 and *P<0.05 compared with the baseline value. ††P<0.01 and **P<0.05 compared with the myoglobin level during the last 15 min of ischemia. ^{a}P<0.01 and ^{b}P<0.05 compared with the corresponding myoglobin level in the VX group.

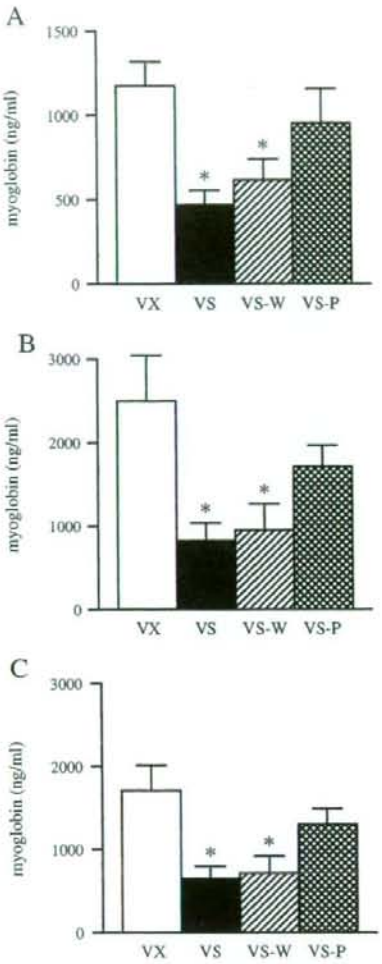

Fig. 2. Average myoglobin levels for the ischemic period (A), reperfusion period (B), and total period throughout ischemia and reperfusion (C). In all panels, the myoglobin levels were significantly lower in the vagal stimulation (VS), and vagal stimulation with wortmannin pretreatment (VS-W) groups than in the control, vagotomized (VX) group. The myoglobin levels in the vagal stimulation with fixed-rate pacing (VS-P) group did not markedly differ from those in the VX group. Data are shown as the means + SE ($n = 6$ each). *$P < 0.05$ compared with the VX group.

arrhythmia scarcely occurred in the present experimental settings. The cardioprotective effect induced by vagal stimulation may include direct effects of ACh on the ischemic myocardium and indirect effects induced through altered hemodynamics.

For the direct effects, ACh administered prior to a coronary artery occlusion can exert a preconditioning mimetic effect via a signaling pathway that includes PI3K (Qin et al., 2003; Oldenburg et al., 2003). Because we initiated vagal stimulation immediately after the LAD occlusion, however, the mechanism underlying the reduced myocardial damage observed in the present study is likely independent of the preconditioning mimetic effect. In support of this interpretation, the inhibition of PI3K did not affect the reduced myoglobin release induced by vagal stimulation (Fig. 2A, VS-W group). The results of the present study, however, did not preclude the direct involvement of ACh through mechanisms other than the PI3K pathway.

For the indirect effects, bradycardia reduces myocardial oxygen consumption by decreasing the number of ventricular contractions per unit time (Sammel et al., 1983; Shinke et al., 1999). Vagal stimulation also dilates normal coronary arteries via ACh and vasoactive intestinal polypeptide release (Feigl, 1969; Reid et al., 1985; Feliciano and Henning, 1998; Henning and Sawmiller, 2001), which may increase collateral flow into the ischemic region. Bradycardia associated with vagal stimulation may increase coronary perfusion due to a prolonged diastolic interval (Buck et al., 1981), reduced ventricular contractility via a force-frequency mechanism (Maughan et al., 1985), and antagonism of the sympathetic effect (Nakayama et al., 2001). These processes may have improved the balance between energy supply and demand, leading to reduced myocardial injury in the ischemic region. In the present study, the VS-P group showed myoglobin levels that were between those of the VX and VS groups (Fig. 2A), suggesting that bradycardia plays a significant role in vagally induced cardioprotection. The observed effect of fixed-rate ventricular pacing on the vagal effect agrees with our previous study (Kawada et al., 2006), in which prevention of bradycardia using ventricular pacing abolished the suppressive effect of vagal stimulation on the ischemia-induced increase in myocardial interstitial norepinephrine levels.

Reperfusion-induced myocardial injury

Reperfusion of the LAD increased the myocardial interstitial myoglobin level compared with that detected during the last 15 min of ischemia (Fig. 1), which agreed with in vivo observations in the rabbit heart (Kitagawa et al., 2005). In the isolated perfused rat heart, 30 min of hypoxia or anoxia increased the concentration of creatinine kinase in the interstitial transudate, an effect that was further augmented by reoxygenation (Wienen and Kammermeier, 1988). The increased levels of these macromolecules upon reperfusion may have resulted from a reperfusion injury. During ischemia, ATP deficiency impairs the operation of Na^+/K^+ ATPases, resulting in the accumulation of intracellular Na^+. Ischemia also causes acidosis in the ischemic region. Upon reperfusion, washing out the excess extracellular H^+ promotes intracellular Na^+ accumulation via Na^+/H^+ exchange. Eventually, Ca^{2+} influx occurs due to reverse-mode operation of Na^+/Ca^{2+} exchangers (Lazdunski et al., 1985). Once the intracellular Ca^{2+} concentration reaches a threshold level, ATP resynthesis causes hypercontracture of myofibrils and cytoskeletal lesions (Piper, 1989; Piper et al., 2004). Additionally, the recovery of myocardial contraction upon reperfusion increases the leakage of

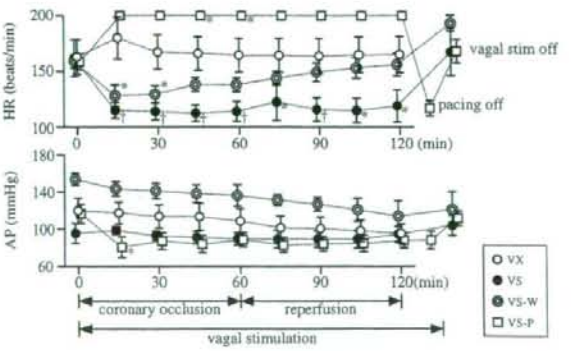

Fig. 3. Changes in heart rate (HR) and arterial pressure (AP). The HR and AP data immediately before the coronary occlusion are shown at time 0. In the vagal stimulation (VX) and vagal stimulation with wortmannin pretreatment (VS-W) groups, cessation of vagal stimulation increased the HR, suggesting that vagal stimulation was effective until the end of the reperfusion period. In the vagal stimulation with fixed-rate pacing group (VS-P), cessation of pacing decreased the HR, whereas cessation of vagal stimulation increased the HR, suggesting that vagal stimulation was effective during ventricular pacing. Data are shown as the means ± SE ($n = 6$ each). †$P < 0.01$ and *$P < 0.05$ compared with the corresponding data from the VX group.

cytosolic molecules from damaged sarcolemmal membranes. For example, ventricular wall stress increases the leakage of lactate dehydrogenase after anoxia in K^+-arrested, isolated, perfused rat heart (Takami et al., 1990). These two explanations are not mutually exclusive and both may contribute to the increased myocardial interstitial myoglobin levels during reperfusion.

In the present study, vagal stimulation significantly reduced the myoglobin levels in the VS and VS-W groups during the reperfusion period (Fig. 2B). The reduced myoglobin levels during the reperfusion period correlated with the decreased myoglobin levels during the ischemic period. It is likely that reduced myocardial injury during the ischemic period contributed to the inhibition of myocardial injury during the reperfusion period. Further studies that include stimulating the vagal nerve during the ischemic or reperfusion period separately may be required to identify the respective effects of vagal stimulation during each of these potentially deleterious events. Although the PI3K signaling pathway played a significant role in the prevention of reperfusion injury by low-pressure reperfusion and postconditioning in the isolated rat heart (Bopassa et al., 2006), the inhibition of PI3K by wortmannin did not antagonize the reduction in myoglobin release induced by vagal stimulation in the present study. The fact that wortmannin inhibits superoxide release from polymorphonuclear leukocytes and exerts cardioprotective effects during myocardial ischemia and reperfusion (Young et al., 2000) makes it difficult to interpret the in vivo effects of wortmannin in blood perfused hearts.

Reperfusion is a pre-requisite to salvaging viable myocardium, following an acute myocardial infarction (Hausenloy and Yellon, 2004). Possible clinical relevance of vagal stimulation is that vagal stimulation may be able to reduce myocardial damage associated with the reperfusion therapy. Endovascular approach (Nabutovsky et al., 2007) may be feasible for vagal stimulation in acute clinical settings. In a long-term treatment, we have shown that intermittent vagal stimulation improves the survival of chronic heart failure following myocardial infarction in rats (Li et al., 2004). On the other hand, bradycardic therapy using a sinus node inhibitor cilobradine also improves left ventricular function and remodeling of chronic heart failure in dogs (Cheng et al., 2007). Although whether bradycardic therapy is equivalent to vagal stimulation remains a matter of investigation, vagal stimulation may be an additional strategy for treatment of myocardial infarction and chronic heart failure.

Limitations

There are several limitations to the present study. First, we did not quantify the infarct size. Although the measurement of myocardial interstitial myoglobin levels are useful to monitor the time course of myocardial injury development, further studies are required to determine the correlation between the local myoglobin levels and infarct size. Second, HR in the VX group declined to approximately 165 beats/min with time elapsed, resulting in the higher HR in the VS-P group than in the VX group. Although the fixed-rate pacing partially reversed the vagally induced protective effect, slowing the pacing rate might have lowered the myoglobin levels in the VS-P group similar to VS group. Finally, while the inhibition of PI3K signaling pathway by pretreatment of wortmannin did not abolish the vagally induced protective effect, expression and/or activation of PI3K signaling pathway components in the ischemic target tissues was not examined. Further studies focusing on the molecular and cellular basis are required to identify the mechanism(s) by which vagal stimulation attenuates the myocardial injury.

Conclusion

Vagal nerve stimulation, initiated immediately after LAD occlusion, reduced myocardial injury as assessed by myocardial interstitial myoglobin levels. The direct effects of ACh on the ischemic myocardium, at least those associated with the PI3K signaling pathway, were not markedly responsible for the vagal stimulation-mediated cardioprotection observed under our experimental conditions. On the other hand, bradycardia played a significant role in the vagal stimulation-induced cardioprotection against acute myocardial ischemia and reperfusion.

Acknowledgments

This study was supported by a Health and Labor Sciences Research Grant for Research on Advanced Medical Technology, a Health and Labor Sciences Research Grant for Research on Medical Devices for Analyzing, Supporting and Substituting the Function of the Human Body, and a Health and Labor Sciences Research Grant H18-Iryo-Ippan-023 from the Ministry of Health, Labour and Welfare of Japan.

References

Akiyama, T., Yamazaki, T., Ninomiya, I., 1994. In vivo detection of endogenous acetylcholine release in cat ventricles. American Journal of Physiology 266 (3 Pt 2), H854–H860.
Bopassa, J.C., Ferrera, R., Gateau-Roesch, O., Couture-Lepetit, E., Ovize, M., 2006. PI 3-kinase regulates the mitochondrial transition pore in controlled reperfusion and postconditioning. Cardiovascular Research 69 (1), 178–185.
Buck, J.D., Warltier, D.C., Hardman, H.F., Gross, G.J., 1981. Effects of sotalol and vagal stimulation on ischemic myocardial blood flow distribution in the canine heart. The Journal of Pharmacology and Experimental Therapeutics 216 (2), 347–351.
Cheng, Y., George, I., Yi, G.H., Reiken, S., Gu, A., Tao, Y.K., Muraskin, J., Qin, S., He, K.L., Hay, I., Yu, K., Oz, M.C., Burkhoff, D., Holmes, J., Wang, J., 2007. Bradycardic therapy improves left ventricular function and remodeling in dogs with coronary embolization-induced chronic heart failure. The Journal of Pharmacology and Experimental Therapeutics 321 (2), 496–476.
Feigl, E.O., 1969. Parasympathetic control of coronary blood flow in dogs. Circulation Research 25 (5), 509–519.
Feliciano, L., Henning, R.J., 1998. Vagal nerve stimulation releases vasoactive intestinal peptide which significantly increases coronary artery blood flow. Cardiovascular Research 40 (1), 45–55.
Glantz, S.A., 2002. Primer of Biostatistics, 5th ed. McGraw-Hill, New York.
Hausenloy, D.J., Yellon, D.M., 2004. New directions for protecting the heart against ischaemia–reperfusion injury: targeting the reperfusion injury salvage kinase (RISK)-pathway. Cardiovascular Research 61 (3), 448–460.
Henning, R.J., Sawmiller, D.R., 2001. Vasoactive intestinal peptide: cardiovascular effects. Cardiovascular Research 49 (1), 27–37.
Kawada, T., Yamazaki, T., Akiyama, T., Mori, H., Inagaki, M., Shishido, T., Takaki, H., Sugimachi, M., Sunagawa, K., 2002. Effects of brief ischaemia on myocardial acetylcholine and noradrenaline levels in anaesthetized cats. Autonomic Neuroscience: Basic and Clinical 95 (1–2), 37–42.
Kawada, T., Yamazaki, T., Akiyama, T., Li, M., Ariumi, H., Mori, H., Sunagawa, K., Sugimachi, M., 2006. Vagal stimulation suppresses ischemia-induced myocardial interstitial norepinephrine release. Life Sciences 78 (8), 882–887.
Kitagawa, H., Yamazaki, T., Akiyama, T., Sugimachi, M., Sunagawa, K., Mori, H., 2005. Microdialysis separately monitors myocardial interstitial myoglobin during ischemia and reperfusion. American Journal of Physiology. Heart and Circulatory Physiology 289 (2), H924–H930.
Lazdunski, M., Frelin, C., Vigne, P., 1985. The sodium/hydrogen exchange system in cardiac cells: its biochemical and pharmacological properties and its role in regulating internal concentrations of sodium and internal pH. Journal of Molecular and Cellular Cardiology 17 (11), 1029–1042.
Li, M., Zheng, C., Sato, T., Kawada, T., Sugimachi, M., Sunagawa, K., 2004. Vagal nerve stimulation markedly improves long-term survival after chronic heart failure in rats. Circulation 109 (1), 120–124.
Maughan, W.L., Sunagawa, K., Burkhoff, D., Graves Jr., W.L., Hunter, W.C., Sagawa, K., 1985. Effect of heart rate on the canine end-systolic pressure–volume relationship. Circulation 72 (3), 654–659.
Myers, R.W., Pearlman, A.S., Hyman, R.M., Goldstein, R.A., Kent, K.M., Goldstein, R.E., Epstein, S.E., 1974. Beneficial effects of vagal stimulation and bradycardia during experimental acute myocardial ischemia. Circulation 49 (5), 943–947.
Nabutovsky, Y., Florio, J., Morgan, K., Grill, W.M., Farazi, T.G., 2007. Lead design and initial applications of a new lead for long-term endovascular vagal stimulation. Pacing and Clinical Electrophysiology 30 (11), S215–S218.
Nakayama, Y., Miyano, H., Shishido, T., Inagaki, M., Kawada, T., Sugimachi, M., Sunagawa, K., 2001. Heart rate-independent vagal effect on end-systolic elastance of the canine left ventricle under various levels of sympathetic tone. Circulation 104 (19), 2277–2279.
Oldenburg, O., Critz, S.D., Cohen, M.V., Downey, J.M., 2003. Acetylcholine-induced production of reactive oxygen species in adult rabbit ventricular myocytes is dependent on phosphatidylinositol 3- and Src-kinase activation and mitochondrial K_{ATP} channel opening. Journal of Molecular and Cellular Cardiology 35 (6), 653–660.
Piper, H.M., 1989. Energy deficiency, calcium overload or oxidative stress: possible causes of irreversible ischemic myocardial injury. Klinische Wochenschrift 67 (9), 465–476.

Piper, H.M., Abdallah, Y., Schäfer, C., 2004. The first minutes of reperfusion: a window of opportunity for cardioprotection. Cardiovascular Research 61 (3), 365–371.
Przyklenk, K., Kloner, R.A., 1995. Low-dose i.v. acetylcholine acts as a "preconditioning-mimetic" in the canine model. Journal of Cardiac Surgery 10 (4), 389–395.
Qin, Q., Downey, J.M., Cohen, M.V., 2003. Acetylcholine but not adenosine triggers preconditioning through PI3-kinase and a tyrosine kinase. American Journal of Physiology. Heart and Circulatory Physiology 284 (2), H727–H734.
Reid, J.V.O., Ito, B.R., Huang, A.H., Buffington, C.W., Feigl, E.O., 1985. Parasympathetic control of transmural coronary blood flow in dogs. American Journal of Physiology 249 (2 Pt 2), H337–H343.
Rosenshtraukh, L., Danilo Jr., P., Anyukhovsky, E.P., Steinberg, S.F., Rybin, V., Brittain-Valenti, K., Molina-Viamonte, V., Rosen, M.R., 1994. Mechanisms for vagal modulation of ventricular repolarization and of coronary occlusion-induced lethal arrhythmias in cats. Circulation Research 75 (4), 722–732.
Sammel, N.L., Norris, R.M., Hughes, C.F., Johnson, R.N., Ashton, N.G., Elliott, R.L., 1983. Severity of canine myocardial infarcts in relation to indices of oxygen demand: preservation of myocardial creatine kinase activity by vagal stimulation and propranolol. Cardiovascular Research 17 (1), 50–60.
Shinke, T., Takeuchi, M., Takaoka, H., Yokoyama, M., 1999. Beneficial effects of heart rate reduction on cardiac mechanics and energetics in patients with left ventricular dysfunction. Japanese Circulation Journal 63 (12), 957–964.
Takami, H., Matsuda, H., Kuki, S., Nishimura, M., Kawashima, Y., Watari, H., Furuya, E., Tagawa, K., 1990. Leakage of cytoplasmic enzymes from rat heart by the stress of cardiac beating after increase in cell membrane fragility by anoxia. Pflügers Archiv 416 (1–2), 144–150.
Vanoli, E., de Ferrari, G.M., Stramba-Badiale, M., Hull Jr., S.S., Foreman, R.D., Schwartz, P.J., 1991. Vagal stimulation and prevention of sudden death in conscious dogs with a healed myocardial infarction. Circulation Research 68 (5), 1471–1481.
Wienen, W., Kammermeier, H., 1988. Intra- and extracellular markers in interstitial transudate of perfused rat hearts. American Journal of Physiology 254 (4 Pt 2), H785–H794.
Young, L.H., Ikeda, Y., Scalia, R., Lefer, A.M., 2000. Wortmannin, a potent antineutrophil agent, exerts cardioprotective effects in myocardial ischemia/reperfusion. The Journal of Pharmacology and Experimental Therapeutics 295 (1), 37–43.

Am J Physiol Heart Circ Physiol 295: H1081–H1089, 2008.
First published June 27, 2008; doi:10.1152/ajpheart.00023.2008.

Muscle mechanoreflex augments arterial baroreflex-mediated dynamic sympathetic response to carotid sinus pressure

Kenta Yamamoto,[1,2] Toru Kawada,[2] Atsunori Kamiya,[2] Hiroshi Takaki,[2] Toshiaki Shishido,[2] Kenji Sunagawa,[3] and Masaru Sugimachi[2]

[1]*Consolidated Research Institute for Advanced Science and Medical Care, Waseda University, Tokyo;* [2]*Department of Cardiovascular Dynamics, Advanced Medical Engineering Center, National Cardiovascular Center Research Institute, Osaka; and* [3]*Department of Cardiovascular Medicine, Graduate School of Medical Sciences, Kyushu University, Fukuoka, Japan*

Submitted 8 January 2008; accepted in final form 19 June 2008

Yamamoto K, Kawada T, Kamiya A, Takaki H, Shishido T, Sunagawa K, Sugimachi M. Muscle mechanoreflex augments arterial baroreflex-mediated dynamic sympathetic response to carotid sinus pressure. *Am J Physiol Heart Circ Physiol* 295: H1081–H1089, 2008. First published June 27, 2008; doi:10.1152/ajpheart.00023.2008.—Although the muscle mechanoreflex is one of the pressor reflexes during exercise, its interaction with dynamic characteristics of the arterial baroreflex remains to be quantitatively analyzed. In anesthetized, vagotomized, and aortic-denervated rabbits ($n = 7$), we randomly perturbed isolated carotid sinus pressure (CSP) using binary white noise while recording renal sympathetic nerve activity (SNA) and arterial pressure (AP). We estimated the transfer functions of the baroreflex neural arc (CSP to SNA) and peripheral arc (SNA to AP) under conditions of control and muscle stretch of the hindlimb (5 kg of tension). The muscle stretch increased the dynamic gain of the neural arc while maintaining the derivative characteristics [gain at 0.01 Hz: 1.0 ± 0.2 vs. 1.4 ± 0.6 arbitrary units (au)/mmHg, gain at 1 Hz: 1.7 ± 0.6 vs. 2.7 ± 1.4 au/mmHg; $P < 0.05$, control vs. stretch]. In contrast, muscle stretch did not affect the peripheral arc. In the time domain, muscle stretch augmented the steady-state response at 50 s (−1.1 ± 0.3 vs. −1.7 ± 0.7 au; $P < 0.05$, control vs. stretch) and negative peak response (−2.1 ± 0.5 vs. −3.1 ± 1.5 au; $P < 0.05$, control vs. stretch) in the SNA step response. A simulation experiment using the results indicated that the muscle mechanoreflex would accelerate the closed-loop AP regulation via the arterial baroreflex.

muscle stretch; transfer function; exercise pressor reflex; exercise; arterial pressure

THE ARTERIAL BAROREFLEX SYSTEM plays an important role in stabilizing arterial pressure (AP) during daily activity. Knowledge of the open-loop static and dynamic characteristics of the arterial baroreflex is essential for a systematic understanding of how the baroreflex system regulates AP. The static characteristics provide information on the operating point of the baroreflex system (19, 34, 48), whereas the dynamic characteristics determine the stability and quickness of the baroreflex system (14, 22, 23). Importantly, many previous studies showed that exercise resets the baroreflex function (3, 5, 6, 29, 30, 32, 35, 36, 40, 45, 47). However, only a few investigations focused on the dynamic characteristics of the arterial baroreflex during exercise (10, 36, 38, 57). The dynamic characteristics of the arterial baroreflex determine how quickly or slowly the system would response to baroreceptor pressure perturbations. Such information cannot be obtained from the static characteristics alone.

The neural mechanisms responsible for changes in the baroreflex function during exercise are considered to be mediated by central command (6, 13, 29, 39, 46) and by afferent inputs from metabolic and mechanical-sensitive skeletal muscle receptors (11, 12, 17, 41, 43, 44, 49). Regarding the static interaction between the muscle mechanoreflex and arterial baroreflex, we performed a baroreflex open-loop study and reported that muscle stretch extended the response range of sympathetic nerve activity (SNA) to baroreceptor pressure input (58, 59). Based on the results, we hypothesized that the activation of the muscle mechanoreflex would augment the dynamic SNA response to baroreceptor pressure input under open-loop conditions. To the best of our knowledge, however, the effects of the muscle mechanoreflex on the dynamic characteristics of the arterial baroreflex have never been reported.

To test the above hypothesis, we identified the dynamic characteristics of the baroreflex during muscle stretch in anesthetized rabbits under baroreflex open-loop conditions (14, 22, 23). The transfer functions from baroreceptor pressure input to SNA (the baroreflex neural arc) and from SNA to AP (the baroreflex peripheral arc) were estimated by a white noise approach (51). The "whiteness" is essential for the system identification of the arterial baroreflex because it is equivalent mathematically to test the system with all possible pressure changes within the frequency range of interest.

METHODS

Surgical preparations. Animals were cared for in strict accordance with the Guiding Principles for the Care and Use of Animals in the Field of Physiological Sciences approved by the Physiological Society of Japan. All protocols were approved by the Animal Subjects Committee of the National Cardiovascular Center. Seven Japanese White rabbits weighing 2.6–3.0 kg were anesthetized via an intravenous injection (2 ml/kg) of a mixture of urethane (250 mg/ml) and α-chloralose (40 mg/ml) and were mechanically ventilated with oxygen-enriched room air. Supplemental anesthetics (0.2–0.3 ml·kg^{-1}·h^{-1}) were administered continuously to maintain stable AP and heart rate levels during intervals of experimental protocols, which were indicative of an appropriate level of anesthesia. Arterial blood was sampled from the left common carotid artery. Rabbits were slightly hyperventilated to suppress chemoreflexes (arterial P_{CO_2} ranged from 30 to 35 mmHg, arterial $P_{O_2} > 300$ mmHg). Arterial blood pH was within the

Address for reprint requests and other correspondence: K. Yamamoto, Consolidated Research Institute for Advanced Science and Medical Care, Waseda Univ., 513 Wasedatsurumakicho, Shinjuku, Tokyo 162-0041, Japan (e-mail: kenta@aoni.waseda.jp).

The costs of publication of this article were defrayed in part by the payment of page charges. The article must therefore be hereby marked "*advertisement*" in accordance with 18 U.S.C. Section 1734 solely to indicate this fact.

physiological range when examined at the end of the surgical preparation as well as at the end of the experiment. The body temperature of each animal was maintained at ~38°C with a heating pad. AP was measured using a high-fidelity pressure transducer (Millar Instruments, Houston, TX) inserted from the right femoral artery to the aortic arch.

We isolated bilateral carotid sinuses from the systemic circulation by ligating the internal and external carotid arteries and other small branches originating from the carotid sinus region. Isolated carotid sinuses were filled with warmed physiological saline via catheters inserted through the common carotid arteries. Intra-CSP was controlled by a servo-controlled piston pump (model ET-126A, Labworks, Costa Mesa, CA). Bilateral vagal and aortic depressor nerves were sectioned at the neck to minimize reflexes from the cardiopulmonary region and from the aortic arch.

We exposed the left renal sympathetic nerve retroperitoneally and attached a pair of stainless steel wire electrodes (Bioflex wire AS633, Cooner Wire, Chatsworth, CA) to record SNA. The nerve bundle peripheral to the electrodes was tightly ligated and crushed to eliminate afferent signals from the kidney. The nerve and electrodes were secured with silicone glue (Kwik-Sil, World Precision Instruments, Sarasota, FL). The preamplified nerve signal was band-pass filtered at 150–1,000 Hz, full-wave rectified, and low-pass filtered with a cutoff frequency of 30 Hz to quantify the nerve activity.

With the rabbit in the prone position, the sacrum, left ankle, and knee were clamped with a custom-made apparatus to prevent body trunk and hindlimb movement during muscle stretch. The left triceps surae muscle, Achilles tendon, and calcaneus bone were exposed. The left triceps surae muscle was isolated from the surrounding tissue. The Achilles tendon was severed from the calcaneus bone and attached to a force transducer (Load Cell LUR-A-SA1, Kyowa Electronic Instruments, Tokyo, Japan). During muscle stretch, the other side of the force transducer was connected to a 5-kg weight via a pulley.

Protocols. To obtain operating pressure values, the carotid sinus baroreflex negative feedback loop was effectively closed by adjusting CSP to AP. Mean AP (and thus mean CSP) at steady state was treated as the operating pressure under control conditions. We then performed muscle stretch for 1 min while the carotid sinus baroreflex was effectively closed. Mean AP during the last 10 s of muscle stretch was treated as the operating pressure under muscle stretch conditions.

To estimate the baroreflex dynamic characteristics, CSP was assigned either high (+20 mmHg) or low (−20 mmHg) pressure values around the operating pressure according to a binary white noise sequence. The switching interval of the binary white noise signal was set at 500 ms so that the CSP power spectrum was fairly flat up to 1 Hz. We confirmed that the muscle stretch produced a sustained SNA increase for at least 7 min (58). To limit the maximum duration of muscle stretch within this time period, a 6-min CSP perturbation was performed twice using different binary sequences, and the two sets of data were pooled for analyses under both control and muscle stretch conditions. The order of control and muscle stretch conditions was randomized across the animals.

Data analysis. We recorded CSP, muscle tension, SNA, and AP at a sampling rate of 200 Hz using a 12-bit analog-to-digital converter. Data were stored on a dedicated laboratory computer system.

To estimate the neural arc transfer function of the carotid sinus baroreflex, we treated CSP as the input and SNA as the output of the system. In the peripheral arc transfer function, we treated SNA as the input and AP as the output of the system. In the total loop transfer function, we treated CSP as the input and AP as the output of the system. Data analysis was started from 90 s after the initiation of each trial to process the stationary portion of data without the effects of transition from closed-loop CSP waveform to open-loop binary white noise CSP input and the transition from nonstretch to stretch of muscle mechanoreceptors. The input-output data pairs were resampled at 10 Hz and segmented into 50%-overlapping bins of 1,024 points each. For each segment, a linear trend was subtracted, and a Hanning window was applied. A fast Fourier transform was performed to obtain the frequency spectra of the input and output signals. The ensemble averages of input power spectral density [$S_{XX}(f)$], output power spectral density [$S_{YY}(f)$], and cross-spectral density between the input and output [$S_{YX}(f)$] were obtained over eight segments derived from two sets of data, where f represents frequency. Finally, we calculated the transfer function from input to output [$H(f)$] using the following equation (27):

$$H(f) = \frac{S_{YX}(f)}{S_{XX}(f)} \quad (1)$$

Hereinafter, we denote the modulus as the dynamic gain of the transfer function. To quantify the linear dependence between input and output signals in the frequency domain, we calculated a magnitude-squared coherence function [Coh(f)] using the following equation (27):

$$\mathrm{Coh}(f) = \frac{|S_{YX}(f)|^2}{S_{XX}(f)S_{YY}(f)} \quad (2)$$

The coherence value ranges from zero to unity. Unity coherence indicates perfect linear dependence between input and output signals, whereas zero coherence indicates total independence between the two signals.

To facilitate an intuitive understanding of the transfer function, the step response corresponding to the transfer function was also calculated as follows. The system impulse response was derived from the inverse Fourier transform of $H(f)$. The step response was obtained from the time integral of the impulse response.

Statistical analysis. All data are presented as means ± SD. Because the amplitude of SNA varied depending on recording conditions, such as the physical contact between the nerve and electrodes, SNA was presented in arbitrary units (au). Neural and peripheral arc transfer functions were normalized in each animal so that the average gain values below 0.03 Hz in the control trial became unity. To compare the transfer functions between two conditions, a transfer gain value at 0.01 Hz ($G_{0.01}$), 0.1 Hz ($G_{0.1}$), 0.5 Hz ($G_{0.5}$), and 1 Hz (G_1) were calculated. In the step response of the neural arc, the steady-state step response at 50 s (S_{50}), the negative peak value (S_{peak}), and the time to negative peak (T_{peak}) were calculated. The effects of muscle stretch on these parameters were examined using the paired t-test. Differences were considered significant when $P < 0.05$.

RESULTS

Figure 1 shows a typical time series of CSP, muscle tension, SNA, and AP under control (*left*) and muscle stretch (*right*) conditions. Although the same binary sequence was applied for two conditions in each animal, different binary sequences were applied for different animals to reduce possible systematic errors in system identification caused by a bias in whiteness specific to a selected binary sequence. The mean CSP during muscle stretch conditions (Fig. 1, *right*) was set higher than that during the control conditions (Fig. 1, *left*) to mimic the increase in the operating pressure during muscle stretch under baroreflex closed-loop conditions (i.e., the AP increase by muscle stretch increases the mean input pressure to the baroreceptors). Muscle stretch increased mean levels of SNA and AP compared with control conditions during the experiment (Table 1).

Figure 2 shows the transfer functions of the neural (*left*) and peripheral (*right*) arcs estimated under the control and muscle stretch conditions; gain plots (*top*), phase plots (*middle*), and Coh(f) (*bottom*) are also presented. The thin and thick solid lines in Fig. 2 indicate control and muscle stretch conditions, respectively. In the neural arc, the dynamic gain increased as